Limits to reconstructing paleotopography from thermochronometer data

Stephanie M. Olen,[1,2] Todd A. Ehlers,[3] and Mathew S. Densmore[1]

Received 9 February 2011; revised 18 December 2011; accepted 14 January 2012; published 16 March 2012.

[1] Recent studies suggest that orogens can achieve a topographic steady state whereby equilibrium is reached between tectonics and erosion. However, steady state topography may not be the norm in many orogens experiencing large changes in climate or tectonics, which can produce topographic transients. The quantification of transient topography over geologic timescales requires reconstructing paleotopography, but this has proven difficult in many cases. This study investigates the utility of bedrock thermochronometer data to reconstruct orogen paleotopography over million year timescales. Apatite (U-Th)/He and fission track ages are integrated with a thermokinematic model for a single-parameter inversion of paleotopography. An iterative scheme is used that minimizes the misfit between predicted and observed cooling ages to identify the range of paleotopographies that could produce observed ages within sample uncertainty. Two approaches are considered. First, synthetic 2-D topographies are used to test the robustness of the approach. The following topographic evolution scenarios are considered: (1) lateral ridge migration, (2) topographic relief change, and (3) valley widening and deepening from glaciation. Second, the method is applied in three dimensions to existing data from the Coast Mountains of British Columbia, Canada. Results from both applications of the model suggest that (1) paleotopographic reconstruction will typically underpredict the magnitude of topographic change, especially relief change; (2) paleotopography is most successfully reconstructed after lateral ridge migration in long-wavelength topographies; and (3) reconstructed paleotopography from the Coast Mountains, British Columbia, suggests that glacial erosion may have the potential to remove drainage divides and laterally shift topographic ridges and peaks.

Citation: Olen, S. M., T. A. Ehlers, and M. S. Densmore (2012), Limits to reconstructing paleotopography from thermochronometer data, *J. Geophys. Res.*, *117*, F01024, doi:10.1029/2011JF001985.

1. Introduction

[2] Orogen topography evolves from tectonic processes that uplift rock and surface processes that remove it. Previous modeling studies have suggested that tectonic and erosion processes can evolve toward an equilibrium and result in topographic steady state [e.g., *Kooi and Beaumont*, 1996; *Braun and Sambridge*, 1997; *Willett and Brandon*, 2002]. However, large changes in tectonics or climate, such as a climate-induced change in erosion [*Roe and Lindzen*, 2001; *Willett et al.*, 2006; *Whipple*, 2009; *Ehlers and Poulsen*, 2009; *Insel et al.*, 2009], have potential to produce topographic transients. Quantifying paleotopography over geologic timescales has proven difficult, with limited types of data sensitive to transient topography. Low-temperature thermochronometry has been proposed as one tool to quantify the rates and magnitudes of orogen deformation and topographic evolution [e.g., *House et al.*, 1998]. The (U-Th)/He (AHe) and fission track (AFT) thermochronometer systems on apatite have effective closure temperatures of ~70°C and ~110°C, respectively [*Farley*, 2002], and are sensitive to upper crustal (~2–5 km depth) rock cooling histories [e.g., *Ehlers*, 2005]. At these shallow crustal depths, the geometry of subsurface isotherms represents a dampened version of the overlying topography [*Lees*, 1910; *Stüwe et al.*, 1994; *Braun*, 2002a; *Ehlers and Farley*, 2003; *Braun and Robert*, 2005]. If topographic change of sufficient amplitude and wavelength [*Stüwe et al.*, 1994] occurs, a detectable change in the geometry of the closure isotherms can also occur. Thermochronometer samples collected across the present-day topography can contain a record of paleoclosure isotherm geometry and paleotopography at the time of sample cooling. This study builds upon previous work [e.g., *Braun*, 2002a; *Ehlers and Farley*, 2003; *Densmore et al.*, 2007; *Densmore*,

[1]Department of Geological Sciences, University of Michigan, Ann Arbor, Michigan, USA.
[2]Now at Institute of Earth and Environmental Science, University of Potsdam, Potsdam, Germany.
[3]Department of Geosciences, University of Tübingen, Tübingen, Germany.

0148-0227/12/2011JF001985

2008; *Valla et al.*, 2010] and explores the pattern and magnitude of topographic evolution that can be quantified with low-temperature thermochronometer data.

[3] Large topographic changes at the surface are required to produce variations in isotherm geometry detectable with thermochronometry [e.g., *Braun*, 2005]. Given this, previous applications of thermochronometry to orogen evolution have focused on areas where either large magnitudes of fluvial incision have occurred or in heavily glaciated orogens [e.g., *House et al.*, 1998, 2001; *Ehlers and Farley*, 2003; *Braun and Robert*, 2005; *Thiede et al.*, 2005, 2009; *Ehlers et al.*, 2006; *Huntington et al.*, 2006; *Rahl et al.*, 2007; *Schildgen et al.*, 2009, 2010; *Whipp et al.*, 2009; *van der Beek et al.*, 2010]. These studies have documented large transients and/or spatial variations in denudation during orogen evolution. In fluvially dominated landscapes, thermochronometry has been used to quantify the rates and timing of river incision and relief change, for instance in the Sierra Nevada Mountains of California and the eastern flank of the Peruvian Andes [e.g., *House et al.*, 1998, 2001; *Schildgen et al.*, 2009, 2010]. Previous applications of low-temperature thermochronology to glaciated orogens have constrained temporal and spatial variations of glacial erosion [e.g., *Spotila et al.*, 2004; *Shuster et al.*, 2005; *Ehlers et al.*, 2006; *Enkelmann et al.*, 2008, 2009]. Most previous studies have focused on case-study applications of thermochronometry to quantify topographic change in different orogens. With the exception of work by *Braun* [2002a], *Braun and Robert* [2005], *Whipp et al.* [2009], *Valla et al.* [2010], and *Bao et al.* [2011], few studies have evaluated the general response of thermochronometer data to different patterns of topographic evolution.

[4] This study complements previous work by exploring the sensitivity of thermochronometer data to reconstruct paleotopography in landscapes evolving by fluvial and glacial processes. More specifically, this study (1) presents a new iterative single-parameter inversion method for reconstructing paleotopography by minimizing the misfit between observed and predicted cooling ages; (2) explores the sensitivity of the AHe and AFT systems to changes in topography resulting from phase change (lateral ridge migration), relief change, and glaciation (valley deepening and widening) using a series of idealized 2-D topographic profiles; and (3) applies the iterative method in three dimensions to a large existing AHe and AFT data set from the Coast Mountains, British Columbia, to reconstruct the preglacial paleotopography of the region.

2. Background to AHe Thermochronometry and Topography

[5] AHe thermochronometry is increasingly used in tectonic and surface process studies due to the relative abundance of apatite in crustal rocks, the moderately high U-Th content of apatite, and the sensitivity of the system to near-surface rates of faulting and erosion. Apatite crystals are dated by measuring the ingrowth of ^{4}He resulting from alpha decay from U-Th. ^{4}He is retained in samples at effective closure temperatures below ~70–75°C (for a nominal cooling rate of 10°C Myr^{-1}) [*Farley*, 2000]. Similarly, for AFT, fission tracks in apatite are only retained below the annealing, or closure, temperature of ~110°C [*Ketcham*, 2005]. Recorded AHe and AFT ages document the length of time that has elapsed since the sample passed through a closure isotherm [*Dodson*, 1973] while transiting through a partial retention or partial annealing zone. A suite of AHe ages collected across the land surface is sensitive to spatial variations in thermal gradients caused by the overlying topography [e.g., *Lees*, 1910; *Ehlers and Farley*, 2003]. This sensitivity comes from isotherms mimicking the overlying topography with the amplitude of an isotherm's topographic impression decreasing with depth. The low closure temperature of AHe, and to a lesser extent of AFT, is shallow enough in many settings for cooling ages across valleys and ridges to reflect differences in thermal gradients and closure temperature depth. This sensitivity makes it possible to use AHe data to infer the existence and evolution of paleotopography [e.g., *House et al.*, 1998, 2001]. The sensitivity of subsurface isotherms to topography is greatest for low mean exhumation rates (e.g., <~1 km Myr^{-1}) [*Stüwe et al.*, 1994; *Valla et al.*, 2010].

3. Methods

[6] This study uses a modified version (Pecube-D) [*Whipp et al.*, 2009] of the numerical model Pecube [*Braun*, 2002a, 2002b, 2003]. This program is a 3-D transient thermokinematic and erosion model for interpreting bedrock and detrital (hence the -D) thermochronometer data. The model is used to quantify the thermochronometer age response to changing topography. Pecube-predicted ages are used to iteratively solve for paleotopography until the misfit between observed and predicted ages is sufficiently minimized (Figure 1), as described in section 3.2.2.

3.1. Thermokinematic and Age Prediction Model

[7] Pecube-D is a 3-D finite element thermokinematic model that solves the transient advection-diffusion equation as a function of evolving topography, exhumation rate, and thermophysical properties [*Braun*, 2003]. Thermal histories computed for each sample location on the final topography are used to predict cooling-rate-dependent thermochronometer ages at the surface (section 3.1.1). Figure 2 shows an example of the model geometry and setup used in the application to the Coast Mountains of British Columbia.

3.1.1. Age Prediction Model

[8] Thermochronometer ages are predicted at the surface of the modern topography using individual sample cooling histories from the thermal model (section 3.1.2). For 2-D simulations using synthetic data, AHe ages are calculated based on the Durango apatite behavior [*Farley*, 2000]. AFT ages are computed using a multikinetic annealing model [*Ketcham*, 2005; *Ehlers et al.*, 2005].

3.1.2. Pecube Parameterization

[9] Material properties, initial and boundary conditions used in the thermal model are as follows (see Table 1). The model block has a crustal thickness of 40 km with a constant basal temperature of 800°C [cf. *Ehlers et al.*, 2006; *Densmore et al.*, 2007]. Thermophysical property values typical of continental crust are used as model input. Thermal conductivity of the crust is held constant at 2.5 W m^{-1} K^{-1} and the specific heat is set at 1000 J kg^{-1} K^{-1} [*Waples and Waples*, 2004]. Crustal and mantle densities are 2700 kg m^{-3} and 3200 kg m^{-3}, respectively, with a surface heat production of 1.0 μW m^{-3} and a constant mantle heat

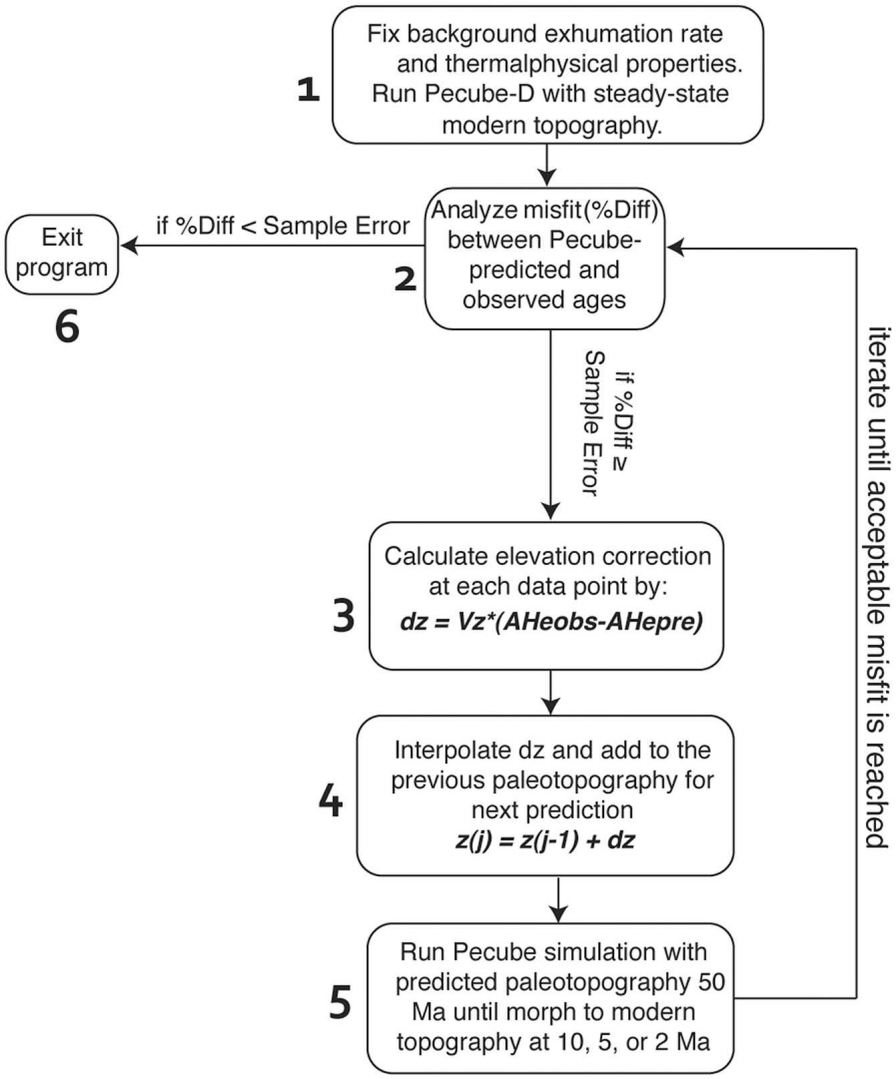

Figure 1. Program flowchart of the proposed iterative method for reconstructing paleotopography. The program begins by predicting AHe ages on a steady state modern topography (step 1); a misfit calculation is then performed; if the percent difference between observed and predicted ages is greater than the sample error, proceed to steps 2–5 to calculate paleotopography until the predicted ages fit within the sample error of observed ages or until a critical number of iterations has been reached. See section 3.2.2 for details of misfit minimization.

production of 0.1 μW m^{-3} [*Pinet et al.*, 1991]. Crustal radiogenic heat production decreases exponentially with depth from the surface value with an *e*-folding depth of 10 km [e.g., *Lachenbruch*, 1970]. Temperature at the lowest surface elevation in the topography is set to 10°C, with an atmospheric lapse rate of −6.5°C km^{-1}. Thermophysical properties are held constant in all iterations and simulations.

3.2. Iterative Topographic Reconstruction

[10] The method presented here uses thermochronometer data collected across the topography to iteratively solve for (i.e., invert) paleotopography by evolving topography to minimize the misfit between predicted and observed ages. Uncertainties in the sample cooling ages are accounted for and used to determine the range of paleotopographies that could have produced an observed pattern in cooling ages. The iterative method for predicting paleotopography has two components: (1) an inversion of AHe data to calculate an elevation correction (paleotopography) at each sample location and (2) a misfit reduction measure to control the iterative scheme. Figure 1 demonstrates how these two elements work together to produce a final prediction of paleotopography. An overview of the modeling procedure is as follows (Figure 1): (1) an initial forward model simulation is run using steady state modern topography and a uniform prescribed background exhumation rate to predict AHe ages (e.g., Figure 2); (2) the misfit between model-predicted and observed AHe ages is calculated; (3) a correction is applied to the elevation of sample locations (and hence topography) using the misfit in ages from step 2 and the model exhumation rate defined in step 1; this step provides a new initial paleotopography used in the next iteration; (4) a subsequent forward model simulation is run using the modified topography from the previous step as the initial topography; this

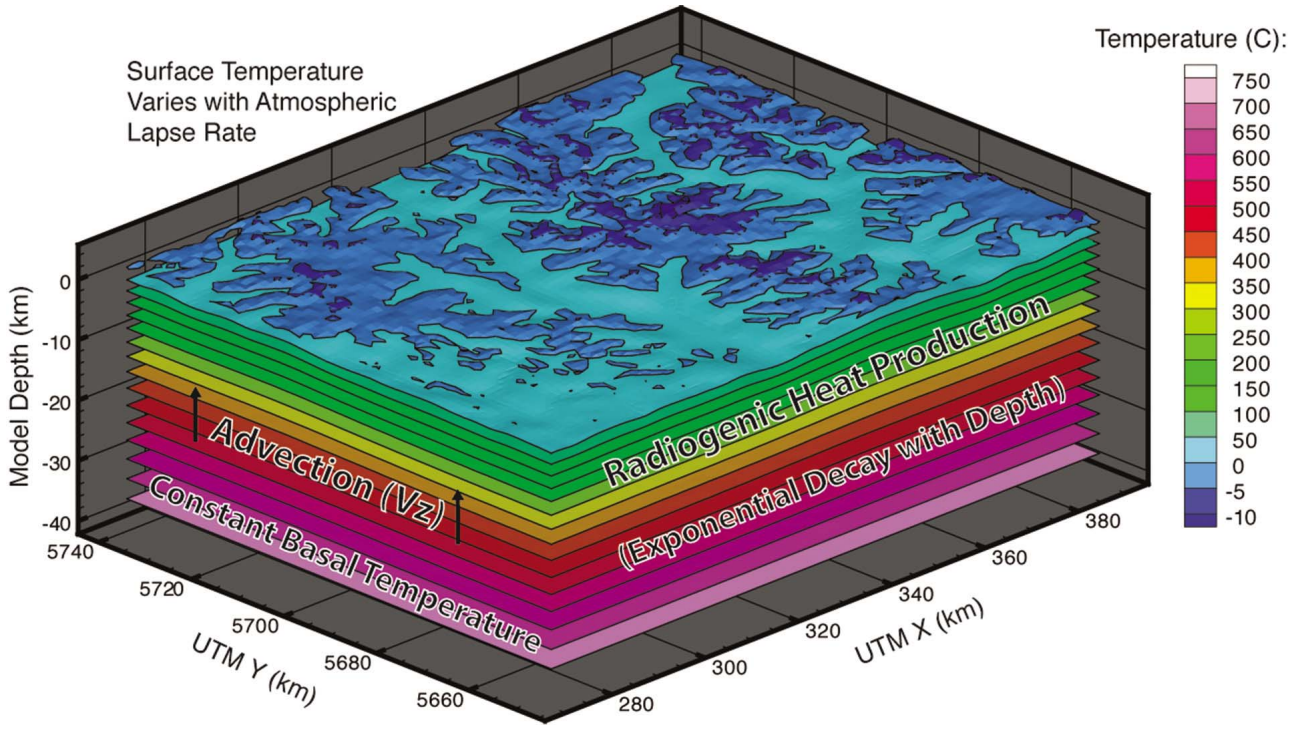

Figure 2. An example block diagram showing isotherms below a complex alpine topography (Mount Waddington, Coast Mountains, British Columbia) generated using Pecube-D. Heat is advected from the mantle by tectonically driven rock uplift and is generated in the crust by radiogenic decay, decreasing exponentially with depth. The surface temperature at sea level is 10°C; temperature decreases with elevation by an atmospheric lapse rate of 6.5°C km^{-1}.

estimated paleotopography then evolves toward the present-day topography over a user defined time interval; (5) predicted AHe ages on the present-day topography are again calculated as a function of the sample cooling histories calculated from step 4; and (6) steps 2 through 5 are repeated until the misfit between the predicted and observed ages is sufficiently minimized (e.g., Figure 3). Best fit models are defined, and model iteration stops, when the ages predicted using the reconstructed paleotopography are within sample error of the observed ages.

[11] By iteratively comparing ages and predicting paleotopography, estimations are refined until predicted ages are within sample error of the observed ages. The approach used here is the simplest (brute force) approach that can be used to invert for paleotopography. This approach assumes that the entire misfit between predicted and observed ages at each sample location is due to a single parameter of topographic change and is therefore limited in its applicability, and is not suitable for settings with nonuniform background exhumation (e.g., faulting, see also section 5). Details of how this minimization is performed follow in section 3.2.2.

3.2.1. Calculation of Paleotopography

[12] Thermochronometer ages predicted by the thermokinematic model (steps 1 and 5, Figure 1) are used to calculate a topographic elevation correction. This elevation correction is applied to either (1) modern topography in the first iteration or (2) the previously predicted paleotopography for all subsequent iterations to make an improved prediction of paleotopography. The elevation correction is determined by an inversion of the difference between the

Table 1. Model Fixed and Explored Parameters Used in the Suite of 2-D Model Simulations[a]

Parameter	Value
Model Fixed Parameters	
Initiation of model	50 Ma
Duration of topographic evolution	5 Myr
Uniform background exhumation rate	0.5 km Myr^{-1}
Crustal thickness	40 km
Thermal conductivity	2.5 W m^{-1} K^{-1}
Specific heat capacity	1000 J kg^{-1} K^{-1}
Crustal density	2700 kg m^{-3}
Mantle density	3200 kg m^{-3}
T at base of model	800°C
T at lowest elevation	10°C
Atmospheric lapse rate	6.5°C km^{-1}
Crustal heat production at surface	1.0 μW m^{-3}
e-folding depth	10 km
Mantle heat production	0.1 μW m^{-3}
Model resolution	160 m
Grid size	[variable in *x* direction] × 3
Topographic evolution	linear
Explored Parameters	
Lateral ridge migration (phase change)	$\pi/4$, $\pi/2$, $3\pi/4$, π
Relief change	−1, −0.5, 0.5, 1 km
Glacial valley deepening	0, 0.5, 1 km
Topographic wavelength (Sinusoidal)	10, 20, 35, 50, 75, 100 km
Glacial valley ridge crest-to-crest distance	10, 15, 20, 40 km

[a]Thermophysical properties are based on average values for unfractured granitic crust. The grid size for 2-D simulations varies in the *x* direction to accommodate constant grid resolution. Values of explored parameters were chosen to reflect a range of topographic scenarios from extreme to more geologically realistic settings to test the breadth of the reconstruction method.

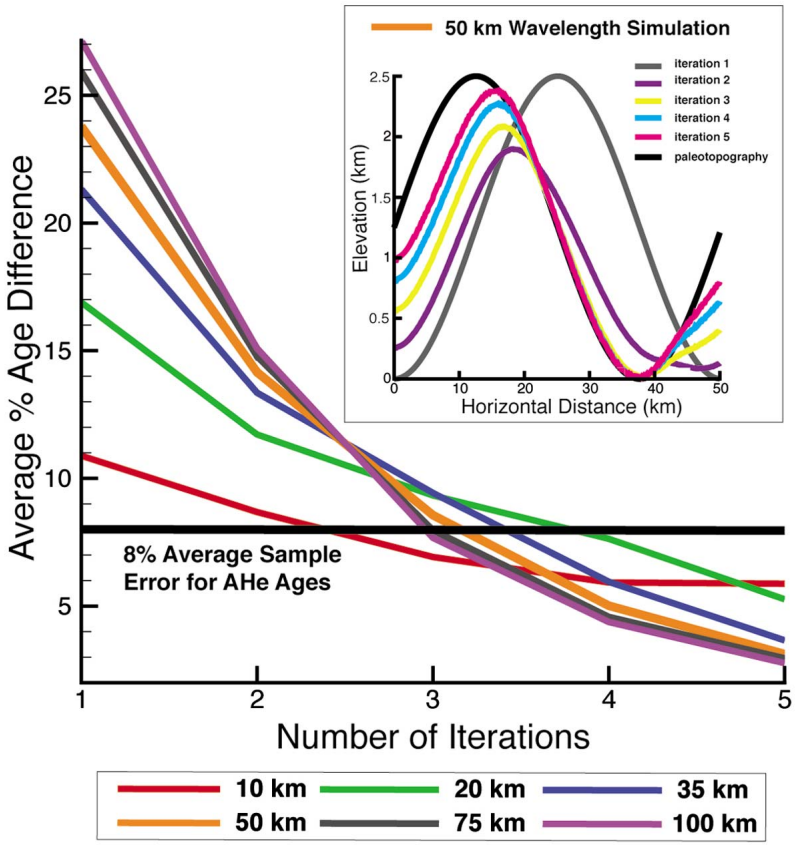

Figure 3. An example of how misfit is reduced over model iterations. Misfit is calculated using the average percent age difference between predicted and observed ages. The best fit to the data is achieved when the calculated percent age difference is less than or equal to the known sample error. Results shown here are from a suite of simulations experiencing a topographic phase shift of $\pi/2$ over 5 Myr. The reduction in the age difference is shown for all wavelengths. The insert for the 50 km wavelength simulation shows the predicted paleotopography at each iteration shown in the primary plot, beginning with the modern topography (iteration 1).

predicted and observed AHe ages and assumes the following relationship between exhumation rate, topography, and time:

$$Vz = \mathrm{d}z/\mathrm{d}t \tag{1}$$

where Vz is the exhumation rate in the vertical direction (km Myr^{-1}), $\mathrm{d}z$ is the change in topography (km) over time $\mathrm{d}t$ (Myr). Assuming a constant background exhumation rate, the topographic change ($\mathrm{d}z$) required to improve the fit to the data is calculated by defining the change in time ($\mathrm{d}t$) as the difference between the observed and predicted AHe ages. The elevation correction for each sample location, for each iteration, is determined by rearranging equation (1):

$$\mathrm{d}z = Vz\left(\mathrm{AHe}_{\mathrm{pre}} - \mathrm{AHe}_{\mathrm{obs}}\right) \tag{2}$$

where $\mathrm{AHe}_{\mathrm{pre}}$ is the model-predicted AHe age and $\mathrm{AHe}_{\mathrm{obs}}$ is the observed AHe age. The correction is calculated at each sample location; if the number of data points is less than the number of nodes in the model topography, a bilinear interpolation is performed between sample locations. For the 2-D simulations in this study using synthetic data, observed ages exist at every node in the topography and no interpolation is necessary. A new paleotopography ($z(j)$) is predicted by adding the elevation correction to the previous paleotopography ($z(j-1)$), such that

$$z(j) = z(j-1) + \mathrm{d}z \tag{3}$$

where j is the iteration number. The new paleotopography is used as the initial condition in the subsequent iteration.

3.2.2. Misfit Minimization

[13] The average age misfit between predicted and observed ages at all data points is measured by calculating the average percent difference between the Pecube-predicted ages and the observed ages. The average percent difference (% Diff) is calculated as

$$\%\mathrm{Diff} = [\Sigma|\left(\mathrm{AHe}_{\mathrm{pre}} - \mathrm{AHe}_{\mathrm{obs}}\right)/\mathrm{AHe}_{\mathrm{obs}}|]/N \times 100 \tag{4}$$

where N is the number of samples and the value is summed from 1 to N. This calculation allows for a straightforward comparison between the improvement in ages predicted using transient topographies and known or assumed sample error. For example, assuming an average sample error of 8% on AHe ages, if %Diff >8, then the method has not yet

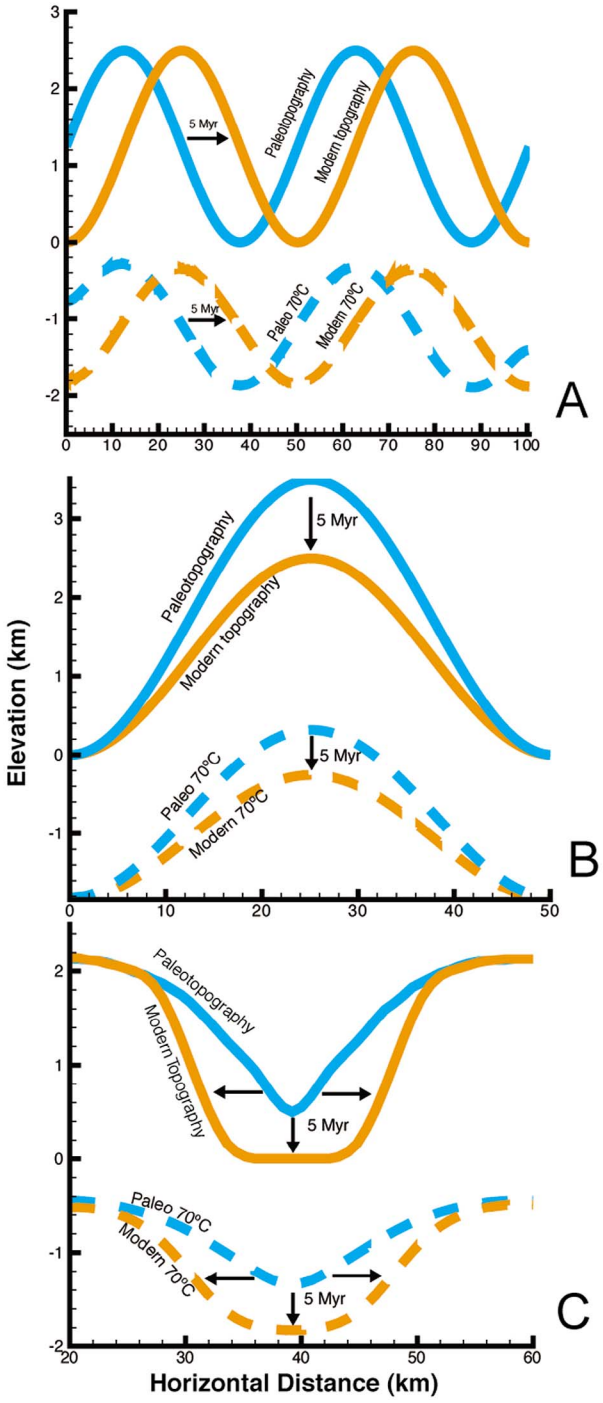

Figure 4. Diagram illustrating the erosional setting of topographic evolution scenarios considered in the 2-D approach: (a) phase shift, (b) relief change, and (c) glacial valley topographic evolution scenarios. Topography is shown (solid) with the corresponding AHe closure isotherm (dashed). A prescribed paleotopography (blue) linearly evolves to the modern topography (orange) over a prescribed time period (5 Myr for all 2-D model simulations). The evolution from paleotopography to modern topography is achieved by differential surface erosion during the last 5 Myr in the thermokinematic model. Ages predicted in the transient topography scenario are used as synthetic data to test the paleotopographic reconstruction method.

reconstructed a good fitting paleotopography. However, when %Diff $\leq$8, the method has predicted a paleotopography that results in AHe ages within the sample error of the data, and we call this a good fit.

[14] The iterative method predicts paleotopography until the average percent difference is within sample error. Simulations in this study assume an AHe sample error of 8%; however, this value could be adjusted to reflect known error on a given data set. Figure 3 shows an example of the misfit reduction and restored paleotopography versus iteration number.

3.3. Sensitivity Analysis to Topographic Change

[15] Three different scenarios for topographic change are considered in this study and are shown in Figure 4: (1) lateral shifting of ridge position, or phase change (Figure 4a), (2) increase and decrease of topographic relief (Figure 4b), and (3) valley deepening and widening due to glaciation (Figure 4c). These scenarios are shown in Figure 4 for example simulations along with the corresponding response of the AHe closure isotherm. A summary of explored and fixed parameters used is found in Table 1. For simulations with a phase or relief change, topographic wavelength is set at 10, 20, 35, 50, 75, and 100 km (Figures 4a and 4b). Phase change is prescribed by values of π and ranges from π, $3\pi/4$, $\pi/2$, and $\pi/4$ for each wavelength (Figure 4a). Topographic relief is altered from paleotopography to modern topography by $\pm$0.5 km and $\pm$1 km for each wavelength (Figure 4b). Phase shift and relief change are considered in isolation of each other. The effects of glacial valley widening and deepening are considered with ridge crest-to-crest distances of 10, 15, 20, and 40 km. Valley widening is constant at 30% of ridge crest distance. Glacial valley deepening of 0, 0.5, and 1 km is considered for each ridge crest distance.

[16] To estimate the range of acceptable paleotopographies for a given data set (see section 3.3.2 for details on how data are synthesized), an envelope of possible paleotopographies is calculated. This is done by adding $\pm 1\sigma$ error (8%) to the observed AHe ages. The reconstruction method is run using the $\pm 1\sigma$ data to predict the upper and lower bounds of potential paleotopographies. The area between these two reconstructions is defined as the envelope of acceptable paleotopographies. It should be noted that because the method always begins with the modern topography and evolves unidirectionally toward a paleotopography, the range of acceptable paleotopographies presented here represents only those that can be generated with this method, and not the full range of topographies that would fit the data. To reconstruct all potential paleotopographies would require running a large suite of simulations each beginning with a different random seed for the initial condition. This would be very computationally costly, however, and the method is only run with the modern topography as an initial condition as the simplest predictor of paleotopography. Future work will investigate the cost-benefit of random seeds of new topography. See section 3.4 for further discussion of this point.

3.3.1. The 2-D Model Setup for Sensitivity Analysis

[17] Paleotopography, calculated using the observed and predicted AHe ages (section 3.2), is used in the kinematic model for simulation times between 50 and 5 Ma. From 5 Ma to present, the landscape evolves linearly from the paleotopography to modern topography. Examples of

topographic change over 5 Myr and the model predicted thermal response of the AHe effective closure isotherm (~70°C) are shown in Figure 4. Other time intervals for the onset of topographic change were also considered (e.g., 10 and 2 Ma). The results presented here characterize the behavior of these other time intervals and for brevity only topographic changes occurring over 5 Ma are shown in Figures 5–11.

[18] The kinematic field used in all simulations is vertical exhumation (Figure 2). A background exhumation rate of 0.5 km Myr^{-1} is applied uniformly across the domain. This value was chosen as a moderate rate of background exhumation in tectonically active orogens. It should be noted that the sensitivity of thermochronometer data to topographic change depends on the magnitude of exhumation [e.g., *Stüwe et al.*, 1994; *Valla et al.*, 2010], but a detailed analysis of thermochronometer sensitivity to other rates is beyond the scope of this study and the focus is instead on topographic evolution scenarios, which has not previously been explored in depth in modeling studies. A brief discussion of the effect of background exhumation rates on the method presented here is given in section 5.3. It should be noted that the total exhumation rate of samples (rate of motion toward the topography) is dependent upon not only this background rate, but also the topographic evolution scenario. The total exhumation rate of samples thus varies spatially across the domain between 5 and 0 Ma to compensate for changes in topography while the landscape is evolving.

3.3.2. Two-Dimensional Data Simulation Setup

[19] Simple one-dimensional, two-period sinusoidal topographies are used for testing the effects of phase (ridge migration) and relief change (Figures 4a and 4b) on AHe and AFT ages. Elevations were sampled from glacial valleys in the Coast Mountains and interpolated using a cubic spline to create simple, idealized glacial and fluvial valleys (Figure 4c). The number of nodes in each topographic wavelength varies to allow for a fixed model resolution of 160 m. Each topography has a depth of three nodes to satisfy the 3-D geometry required in Pecube simulations; the topographic profile is identical across each node in the *y* dimension thereby resulting a 2-D thermal field. Table 1 describes the topographic relief, wavelength, grid size, and model resolution used for 2-D topographies. For all 2-D simulations, synthetic ages are predicted on the final (modern) topography after morphing between paleotopography and modern topography. These ages are treated as "observed" ages, or data, and used in the inverse/iterative simulations to evaluate how well the method reconstructs the paleotopography.

3.4. Model Assumptions, Limitations, and Caveats

[20] Multiple processes influence thermochronometer ages in active orogens. In many cases, it is unlikely that one parameter, such as topography, would change in isolation of others. However, the objective of this study is to document under what conditions paleotopography can be reconstructed. To accomplish this, it is assumed that all other factors remain constant, including the basal temperature, boundary conditions, and other thermophysical properties. An application of the approach presented here to real orogens will require a calibration of the thermal model to the local conditions (e.g., material properties, basal temperature, kinematics, and deformation history). Additionally, the effects of fluid flow on thermochronometer ages [e.g., *Whipp and Ehlers*, 2007] are not explicitly considered here. However, the effects highlighted here for a conduction dominated thermal field would be relevant to many situations where a fluid-dominated thermal field is also present, but additional constraints to the magnitude of thermal power output from hot springs would need to be known for the region [e.g., *Ehlers and Chapman*, 1999].

[21] This method cannot be used to constrain the timing of topographic change or the regional background exhumation rate. These factors, which need to be supplied to the model, must be either obtained using a more computationally costly, multiparameter inversion, additional data, or by testing a range of values in search of a good fit, as is done in our application to the Coast Mountains of British Columbia (see section 5.4).

[22] Topographic reconstructions using this method rely on uniform background exhumation in the region of interest. While such uniform exhumation exists in some orogens, this is not the case in many places. We note, however, that the evolution of topography and erosion is superimposed on top of the background rate such that spatial and temporal variations in exhumation rates are present across the surface of each simulation. This method is not well suited for regions with perturbations to the kinematic or thermal field, such as from faulting or near surface reheating of samples from magmatism. The application of this method is therefore limited to orogens where erosion is the dominant mechanism for sample exhumation and large variations in faulting are not present. As shown in section 5, this assumption can be problematic and spatial gradients in background exhumation rate should be evaluated on an application-by-application basis.

[23] Because this method always assumes present-day topography as the first guess of paleotopography and evolves linearly toward a paleotopography, it should be noted that the method will always predict the minimum amount of topographic change necessary to fit the predicted thermochronometer ages to within error of observed ages. Once predicted ages are within sample error, there is no way to distinguish whether the difference between observed and predicted ages is due to topographic change or to sample uncertainty. Additional uncertainty is generated by the method smoothing topography between data points and because additional smoothing occurs in Pecube via heat diffusion. Therefore, even with perfect data, there will likely be some discrepancy between the predicted and true paleotopography. On a practical basis, however, this uncertainty should not be more significant than analytical sample error.

[24] Finally, we note that this technique assumes a single phase and constant rate of topographic change between a paleotopography and modern topography. The assumption of a single phase of topographic change is made to evaluate if the simplest geologic scenario of topographic change can produce the observed ages. Thus, the approach is best suited for regions where a recent and single pulse of topographic change has occurred (e.g., recent glaciation or a pulse of fluvial erosion). Related to this caveat is a tradeoff in predicted cooling ages that can occur if both the onset time of exhumation and background exhumation rate are variable. This effect is largest when only a single observed

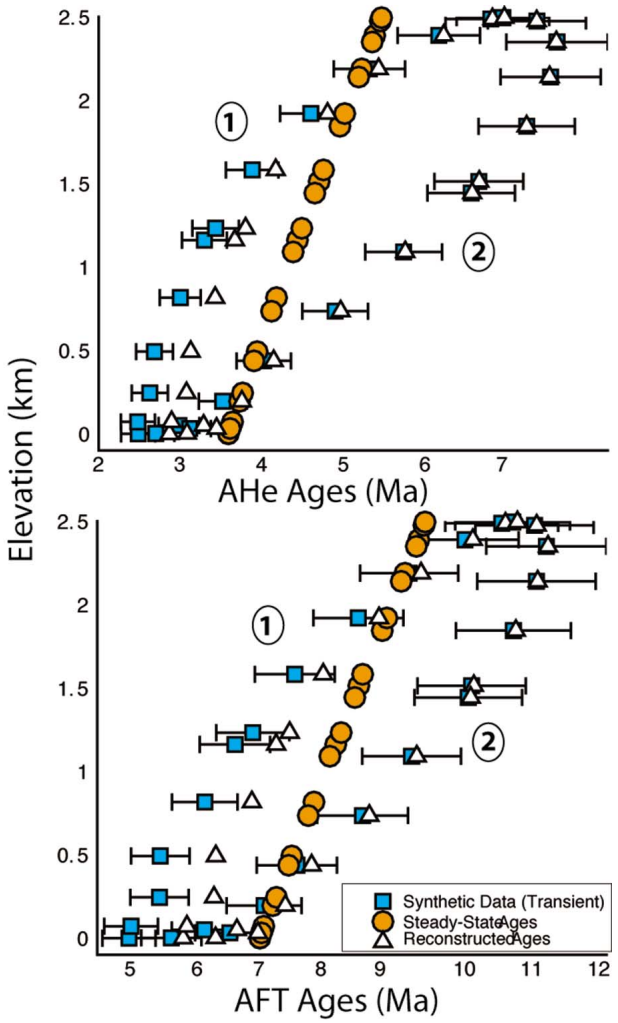

Figure 5. Age-elevation relationship (AER) for (top) AHe and (bottom) AFT ages of an example phase shift simulation. This simulation used synthetic data with a phase shift from paleotopography to modern topography of $\pi/2$; topographic wavelength is 50 km; all topographic changes occur over the last 5 Myr. The looped pattern is the result of different ages on the retreating flank (point 1) and advancing flank (point 2) of the ridge, wherein focused erosion on the retreating flank creates relatively younger ages than on the advancing flank. A prescribed error of 8% was added to the synthetic data to reflect typical 1σ error on AHe data. The AER shows the synthetic data or "observed" ages (blue squares), model-predicted ages on a steady state modern topography (orange circles), and model-predicted ages on the reconstructed transient topography (white triangles). All reconstructions are shown when %Diff ≤8% (assumed sample error).

thermochronometer system is available for comparison to model predictions. In practice, additional geologic knowledge of the onset time of changes in erosion and topography can minimize this effect (e.g., use of multiple thermochronometer systems and/or other geologic evidence such as changes in sedimentation derived from neighboring sedimentary basins). Cases with complex topographic histories are better suited for more sophisticated inverse techniques that evaluate a larger parameter space of topographic change [*Sambridge*, 1999a, 1999b; *Valla et al.*, 2010; *Bao et al.*, 2011].

4. Results

[25] The range of transient topographies investigated requires a minimum of 90 model simulations to analyze the parameters presented in Table 1. The following examines the influence of three types of topographic transients (Figure 4) on AHe and AFT ages and the ability of the model to reconstruct paleotopography under these conditions. In all simulations, AHe ages are used to reconstruct paleotopography and calculate misfit. Age-elevation relationships (AER) for AFT ages are also shown to demonstrate the amount of signal to topographic changes produce in AFT age data. Example illustrative model results are shown here and the full range of model results are presented in section 5. Owing to the fact that this section uses synthesized data, age differences can be almost entirely minimized; however, all predicted paleotopographies and ages are presented when the average percent difference between the observed and predicted ages is equal to or less than sample error (8%) to represent the amount of paleotopographic reconstruction that can be accomplished considering typical data uncertainty.

4.1. Effects of Lateral Ridge Migration on Cooling Ages

[26] Lateral ridge migration (or the phase shift of a sinusoidal topography) can result from several geologic processes, including strong orographic precipitation, glaciations, and/or lateral motion due to thrust faulting. Previous studies [e.g., *Stüwe and Hintermüller*, 2000] have suggested that ridge migration may be detectable using low-temperature thermochronometry. Lateral ridge migration produces a distinguishable signal in both AHe and AFT ages in this study. The AERs for AHe and AFT from a sample synthetic simulation are shown in Figure 5. This simulation was conducted with synthetic data generated from a transient topography with a phase shift of $\pi/2$, or 15 km for a 50 km wavelength, over 5 Myr with topographic relief of 2.5 km (see Table 1 for all fixed parameters). This geometry is similar to orogen perpendicular, long-wavelength topography found in some mountain ranges (e.g., Basin and Range of the western United States). The synthetically produced "observed" ages and the ages predicted on steady state modern topography are shown with the reconstructed age-elevation distribution (Figure 5).

[27] The relationship between age and elevation in orogens is often near linear; here, however, the AER of transient topographies has a looped or two-sided trend, representing the retreating (point 1 on Figure 5 and 6) and advancing (point 2 on Figure 5 and 6) flanks of the migrating ridge. The retreating flank of the ridge has relatively younger ages at a given elevation due to focused erosion compared to the advancing ridge flank, which has comparably older ages at the same elevation. This reproduces the relationship shown by *Stüwe and Hintermüller* [2000] with respect to the "wet" and "dry" side of orographic precipitation-driven ridge migration. This is in contrast to the near linear AER of the steady state modern topography (Figure 5). Figure 5 shows that predicted ages on the steady state topography are more than one standard deviation away from the synthetic data

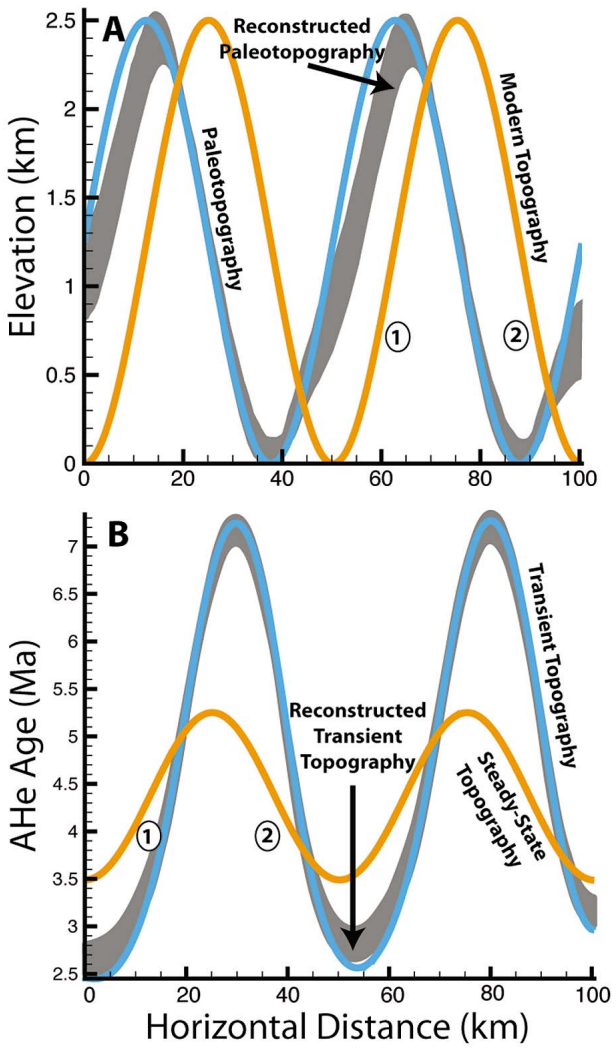

Figure 6. Example profiles of (a) elevation and (b) AHe ages across horizontal distance. Profiles are taken from the same model simulation used in Figure 5 (phase change is $\pi/2$, topographic wavelength is 50 km). The suite of acceptable reconstructed paleotopographies, based on an average 8% error in the age data, is shaded gray (see section 3.3 for details of how this suite was calculated). The looped AER shown in Figure 5 is caused by the left-hand flank of the paleotopography retreating to its modern position (point 1), while the right-hand flank of the paleotopography advances to its modern position (point 2). The resulting asymmetry in ages is shown in Figure 6b.

(initial %Diff = 23.79%), with over 2 Ma age difference at some elevations (e.g., at 2 km). The difference in trend of the AER between transient and steady state topographies and the relatively high initial percent age difference demonstrates the sensitivity of AHe and AFT ages to phase changes, and the potential to reconstruct paleotopography in regions that may have experienced this type of topographic change.

[28] Results indicate that the effect of lateral ridge migration on AHe ages is large enough to enable the reconstruction of paleotopography (see discussion for exceptions). For example, Figure 6a shows a paleotopographic reconstruction across a sinusoidal topography for the same simulation as Figure 5 (phase shift of $\pi/2$). The reconstructed paleotopography is shown as an envelope of potential paleotopographies based on the $\pm 1\sigma$ uncertainty in cooling ages (shaded gray; see section 3.3 for calculation of acceptable paleotopographies). The range of reconstructed paleotopographies lies mostly between the modern and paleotopography because we assume a single phase of topography change between the two topographies. The resulting paleotopography correctly predicts the position of the advancing flank of the ridge, but results in a somewhat narrower topography and does not accurately predict the location of the retreating ridge flank. The peak elevation in the reconstructed paleotopography ranges from approximately 0.3 km lower to 0.1 km higher than the prescribed paleotopography. It should be noted that a lower topography near the bottom of the envelope is more likely to be predicted by this method, as the reconstruction will cease once the predicted paleotopography is within range of acceptable solutions. AHe ages across the topography (Figure 6b) have a larger range in values in the transient topography than in the case of steady state topography, due to increased erosion rates on the retreating flank and decreased erosion on the advancing flank in the last 5 Myr. AHe ages are well-reconstructed across the topography, and while paleotopography does not predict the full topographic relief or the width of individual ridges, the trend and amount of lateral ridge migration are detectable with this method.

4.2. Effects of Topographic Relief Change on Cooling Ages

[29] Topographic relief (the distance from valley bottom to ridge crest) can change in response to variations in erosion rates on valleys and/or ridges. Model simulations in this scenario accommodate relief change by ridge evolution. Transient topographies caused by relief change in this scenario do not appear to have a strong effect on resulting AHe and AFT age elevation profiles. The AERs of observed, modern steady state, and reconstructed AHe and AFT ages are shown in Figure 7. Ages are shown for an example simulation of decreasing relief from paleotopography to modern topography by 1 km, with a 50 km topographic wavelength. A near-linear relationship between age and elevation exists for both modern steady state and transient topographies, with the difference between ages increasing with elevation. The most notable difference between the transient and steady state topographies is the change in the slope of the AER. Steady state modern topography produces a shallower slope (1.4 km Myr^{-1}, $r^2 = 0.99$) and wider range of AHe (3–5 Ma) and AFT (7–9 Ma) ages. Transient topography with decreasing relief produces a steeper AER (3.1 km Myr^{-1}, $r^2 = 0.99$) with a narrower range of AHe (3–4 Ma) and AFT (7–8 Ma) ages. The initial misfit between the synthetic data and the steady state topography model predicted ages is calculated as %Diff = 12.41%. This reduces to %Diff = 1.47% within three iterations when the slope of the AER (2.9 km Myr^{-1}, $r^2 = 1.0$) has increased sufficiently to fit the synthetic data uncertainties (Figure 7). For both the AHe and AFT age distributions, the reconstructed AER remains approximately midway between the modern steady state and the observed age distributions; this suggests that paleotopography can only be partially reconstructed.

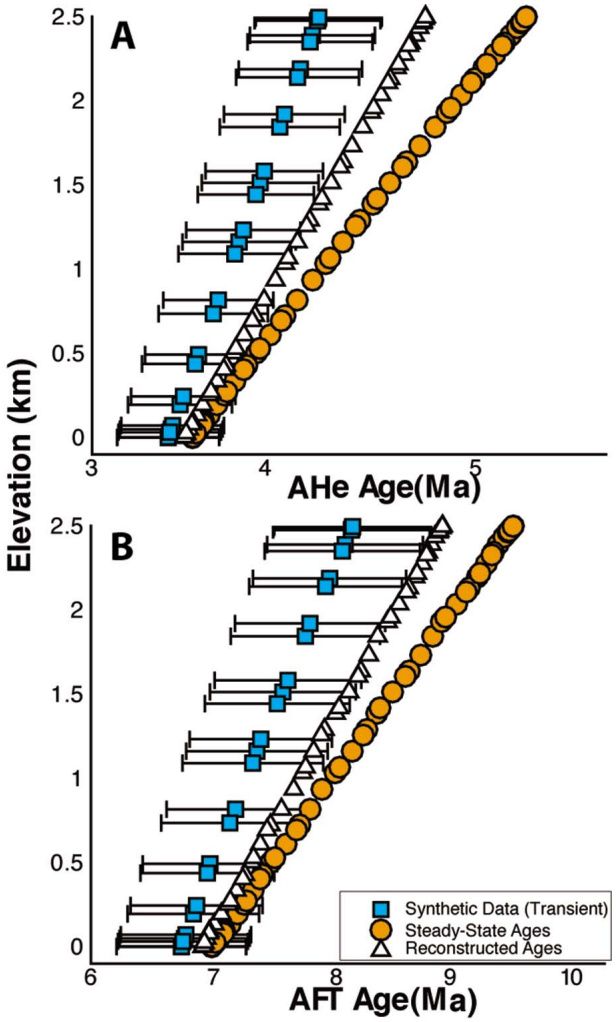

Figure 7. AER for (a) AHe and (b) AFT from an example relief change simulation using a topography with a 50 km wavelength decreasing from 3.5 to 2.5 km over 5 Myr. The AER shows the synthetic data with prescribed 8% sample error (blue squares), model-predicted steady state ages on the modern topography (orange circles), and reconstructed transient ages (white triangles).

[30] The reduced signal produced by topographic relief change coupled with the relatively low number of iterations required to predict ages within sample error of the data, may result in some difficulty fully reconstructing paleotopography. Figure 8 shows profiles of topography (Figure 8a) and AHe age (Figure 8b) across horizontal distance of the sample simulation used in Figure 7. Reconstructed paleotopography is shown as an envelope of acceptable solutions (see section 3.3). The envelope of acceptable paleotopographies extends from "half way" to a full reconstruction of the prescribed paleotopography. However, as in the phase change scenario, the method is most likely to underestimate paleorelief, as the iterative process will likely cease once the reconstructed paleotopography has reached the envelope of acceptable solutions. For example, given the average error prescribed on AHe age data, approximately half of the relief change is reconstructed in this simulation. This amount produces ages young enough to fall within error of the observed ages and stops the iterative process. A reduction in relief results in a younger and narrower distribution of ages across the profile compared to the steady state case (Figure 8b), resulting in a profile that mirrors topography, but with steady state topography AHe ages older than transient topography ages. Predicted topographies and age distributions reproduce the direction of relief change; however, there may not be sufficient signal in the thermochronometer data to reliably reconstruct the amount of increase or decrease in topographic relief. The inverse method here also only reconstructs the minimum possible change in paleotopography within sample uncertainties (see section 3.4) and therefore does not permit a more robust reconstruction.

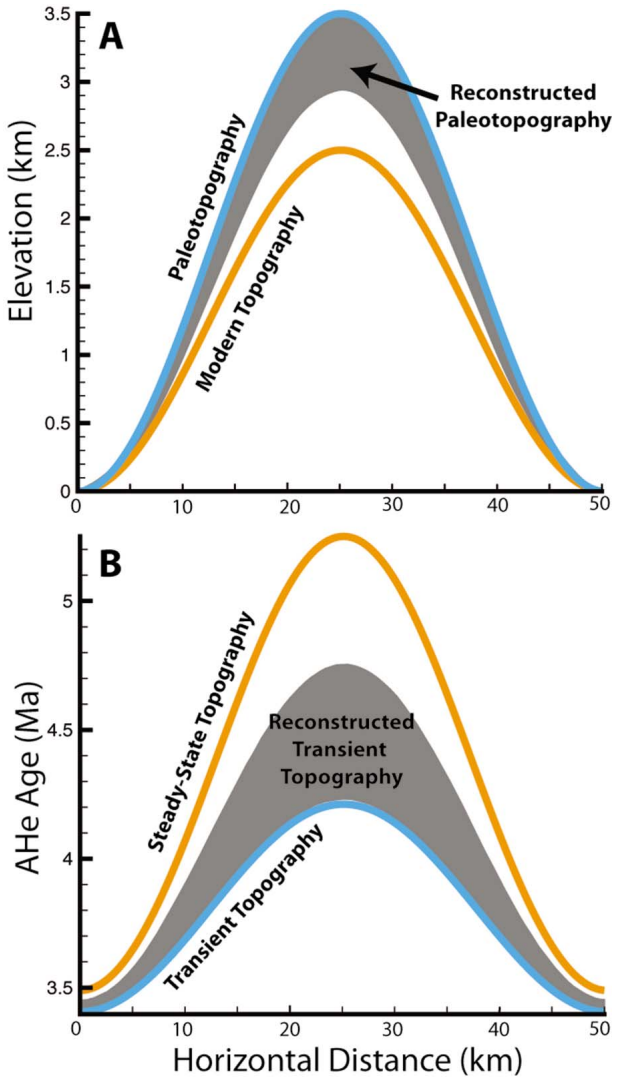

Figure 8. Horizontal profiles of (a) elevation and (b) AHe ages from an example simulation using 50 km topography with reduced relief from 3.5 to 2.5 km over 5 Myr. The suite of acceptable reconstructed paleotopographies, based on an average 8% error in the age data, is shaded gray (see section 3.3 for details of how this suite was calculated).

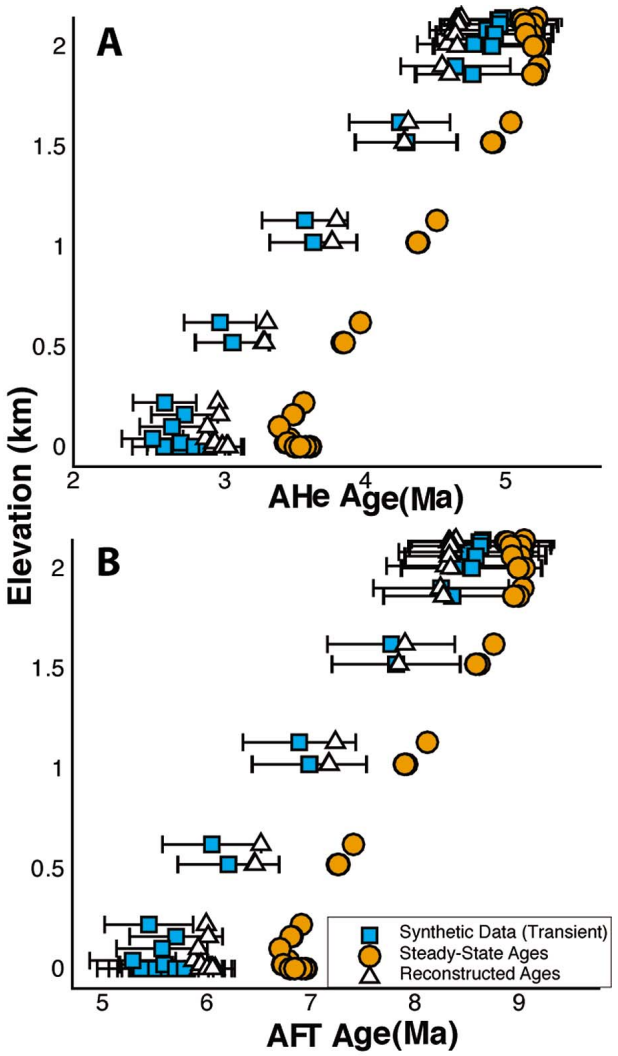

Figure 9. AER for (a) AHe and (b) AFT ages from an example glacial valley erosion simulation using 40 km wavelength topography with 2.5 km relief undergoing 30% valley widening and 1 km relief change. The AER shows synthetic "observed" ages with prescribed 8% error (blue squares), model-predicted steady state ages on the modern topography (orange circles), and reconstructed transient ages (white triangles).

4.3. Effects of Glacial Valley Evolution on Cooling Ages

[31] Glacial valley evolution includes a combination of phase change, the lateral shifting of valley walls, and relief change, deepening of the valley floor (see Figure 4c) [e.g., *Densmore et al.*, 2007]. To allow for relief change to occur only through valley deepening, ridge crests remain fixed in these simulations. Steady state glacial valleys and transient fluvial to glacial valleys produce relatively similar age-elevation relationships. The AERs for steady state glacial "U"-shaped valley and a transient fluvial to glacial ("V" to "U" valley shape, Figure 4c) are shown in Figure 9. Ages are predicted on a 40 km wide ridge crest-to-crest geometry with 2.25 km final relief. The fluvial to glacial valley transient topography simulation prescribes 0.5 km valley deepening and ~30% valley widening. The AERs of both the steady state and transient topographies are nearly linear at moderate elevations, with a wider range of ages at low elevation (valley bottom), particularly in the transient topography. The greatest difference in ages between the simulations is seen along the flanks and on the valley bottom, where valley widening and deepening occur. At higher elevations, similar ages are predicted in the modern steady state and transient case because ridge peaks are not affected by glacial erosion. AER slopes are similar in the two scenarios, with the primary difference being a shift toward younger ages in the transient topography simulation compared to the steady state glacial valley simulation. For example, low elevation (e.g., z = 0 km) ages on the valley floor are ~1 Myr younger for AHe and ~1.5 Myr younger for AFT ages. The lack of large

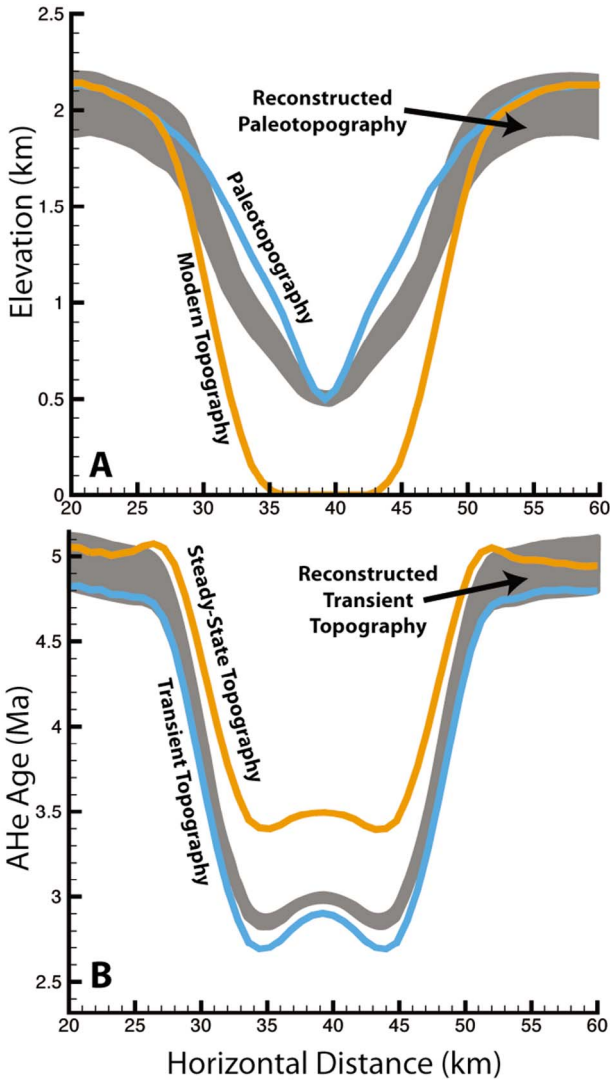

Figure 10. Horizontal profiles of (a) elevation and (b) AHe ages from an example glacial valley evolution simulation using a 40 km topography with 2.5 km relief experiencing 30% valley widening and 0.5 km valley deepening over 5 Myr. The suite of acceptable reconstructed paleotopographies, based on an average 8% error in the age data, is shaded gray (see section 3.3 for details of how this suite was calculated).

age differences is reflected in the initial measure of misfit between the observed ages and the steady state; %Diff = 18.12% for AHe ages; AFT steady state ages are only just out of the range of error of the observed data.

[32] AHe and AFT ages are moderately sensitive to fluvial to glacial valley topographic evolution and paleotopography thus can only be partially reconstructed (Figure 10). The topographic reconstruction is shown as an envelope of acceptable paleotopographies (shaded gray, Figure 10a). The elevation of the valley bottom is correctly predicted and the reconstructed paleotopography has a narrower profile than the modern glacial valley. However, the reconstructed valley remains broader than the "V"-shaped river valley and the method is unable to predict a paleotopography that fully reconstructs the prescribed river valley. AHe ages across the valley profile are shown in Figure 10b. Notable on this profile is the age range across the valley floor, with the youngest ages along the sides of the valley where enhanced erosion has widened the flanks of the fluvial valley. The steady state topography and transient topography have similar ages across the profile, but the transient topography ages are systematically younger, due to the late (last 5 Myr) acceleration in erosion rates in the transient topography. The lack of distinction in AHe ages across the profile complicates the iterative reconstruction of paleotopography, resulting in predicted topographies that do not fully reconstruct the morphology of the prescribed fluvial paleotopography.

5. Discussion

[33] The iterative method presented for reconstructing paleotopography promises to be a useful, but limited, tool for studying transient topographies. A discussion of the sensitivity of the method to the different topographic evolution scenarios, the minimum amount of data required, and the effect of different background exhumation rates is presented here. Following this, the method is applied in three dimensions to the Coast Mountains of British Columbia.

5.1. Sensitivity to Topographic Change in Two-Dimensional Simulations

[34] The sensitivity of AHe ages to the full range of explored parameters (Table 1) is presented in Figure 11. The sensitivity of AHe age data to topographic change is determined by calculating the initial misfit between predicted and observed ages, using predicted ages from the initial steady state modern topography simulation. Model results with an initial average percent difference between steady state and observed ages of less than 8% (assumed sample error) are considered insensitive to the topographic change. In this case, the predicted ages on the modern steady state topography are within sample error of the observed ages and no meaningful paleotopographic reconstruction is possible. Simulations with large initial misfit (e.g., %Diff > 8%) indicate a sufficiently large difference between predicted ages on a steady state modern topography and observed ages to attempt to reconstruct paleotopography.

[35] Model results suggest that AHe cooling ages are most sensitive to lateral ridge migration (phase shift). Figure 11a shows the sensitivity of AHe ages to ridge migration for a range of phase shift values and topographic wavelengths. The greatest sensitivity occurs where there are high magnitudes of lateral ridge migration over large topographic wavelengths. Sensitivity decreases as topographic wavelength and magnitude of ridge migration decrease. For example, for a phase shift of $\pi/2$, the sensitivity of AHe ages increases from an initial %Diff = 10.89% for a 10 km wavelength topography to %Diff = 27.15% for a 100 km wavelength topography. When both the magnitude of phase shift and topographic wavelength become sufficiently small (e.g., a phase shift of $\pi/4$ on a 10 km wavelength topography), the initial sensitivity of AHe ages drops below sample error and prohibits meaningful paleotopographic reconstruction. Dismissing ridge migration of greater than $\pi/2$ as geologically unlikely, the sensitivity of cooling ages suggests that paleotopographic reconstruction is best applied to long-wave topography and ridge-and-valley systems compared to short-wavelength topography, such as small interfluves or individual valleys.

[36] Topographic relief change is less clearly resolved using AHe cooling ages. Figure 11b shows the initial percent difference between ages predicted on steady state modern topography and the synthetic data contoured over the parameter space explored. AHe ages are sensitive to large amounts of relief change (at least 1 km), with little difference between increasing and decreasing relief. Except at the smallest topographic wavelengths (e.g., 10 km) used, topographic wavelength does not have a large effect on the

Figure 11. The sensitivity of AHe age data to (a) lateral ridge migration (phase shift), (b) relief change, and (c) glacial valley evolution contoured over the explored parameter space (the amount of lateral ridge migration and topographic wavelength). Sensitivity is defined as the initial average percent age difference between the synthetic or "observed" ages and steady state ages predicted on a modern topography. The initial misfit must be greater than the 8% assumed sample error to attempt paleotopographic reconstruction. For all scenarios, regions shaded gray indicate that there is not enough initial signal to attempt paleotopographic reconstruction. In Figure 11a the magnitude of lateral ridge migration is expressed in units of π, representing a phase shift on a sinusoidal topography. Changing topographies varied from a slight peak offset ($\pi/4$) to a dramatic (geologically unrealistic) scenario with peaks replacing valleys (π) to test the effectiveness of the method in the most extreme, as well as realistic, scenarios. Sensitivity to ridge migration is lowest when phase shift and topographic wavelength are small, but it is still possible. In Figure 11b, for all relief change simulations, modern topographic relief is 2.5 km; paleotopography ranges from 1.5 to 3.5 km. Paleotopographic reconstruction is not possible in regions where the sensitivity is less than the 8% sample error. This includes all simulations experiencing relief change less than $\sim$0.5 km. In Figure 11c, glacial valley erosion is a combination of valley wall widening, which is constant at $\sim$30% for all simulations, and valley deepening, which varies from 0 to 1 km from an initial 2.5 km relief. Sensitivity is highest in simulations experiencing large amounts of relief change in smaller valleys; this is likely due to glaciers eroding closer to the paleoclosure isotherm in narrower valleys.

sensitivity of ages. Relief change of less than approximately 0.5 km does not produce sufficient signal (%Diff >8%) to allow paleotopographic reconstruction. Paleotopographic reconstructions are only possible for relief change of >0.5 km (for an initial topographic relief of 2.5 km and exhumation rate of 0.5 km Myr^{-1}). Sensitivity is relatively high for increasing relief at low topographic wavelengths compared to decreasing relief (Figure 11b); this is likely because an increase in relief is accompanied by heat advection and incision into or close to the closure isotherm for AHe ages as valley elevation is pinned from paleotopography to modern topography. Where there is sufficient signal, the reconstruction method succeeds in capturing the direction of topographic relief change. However, AHe

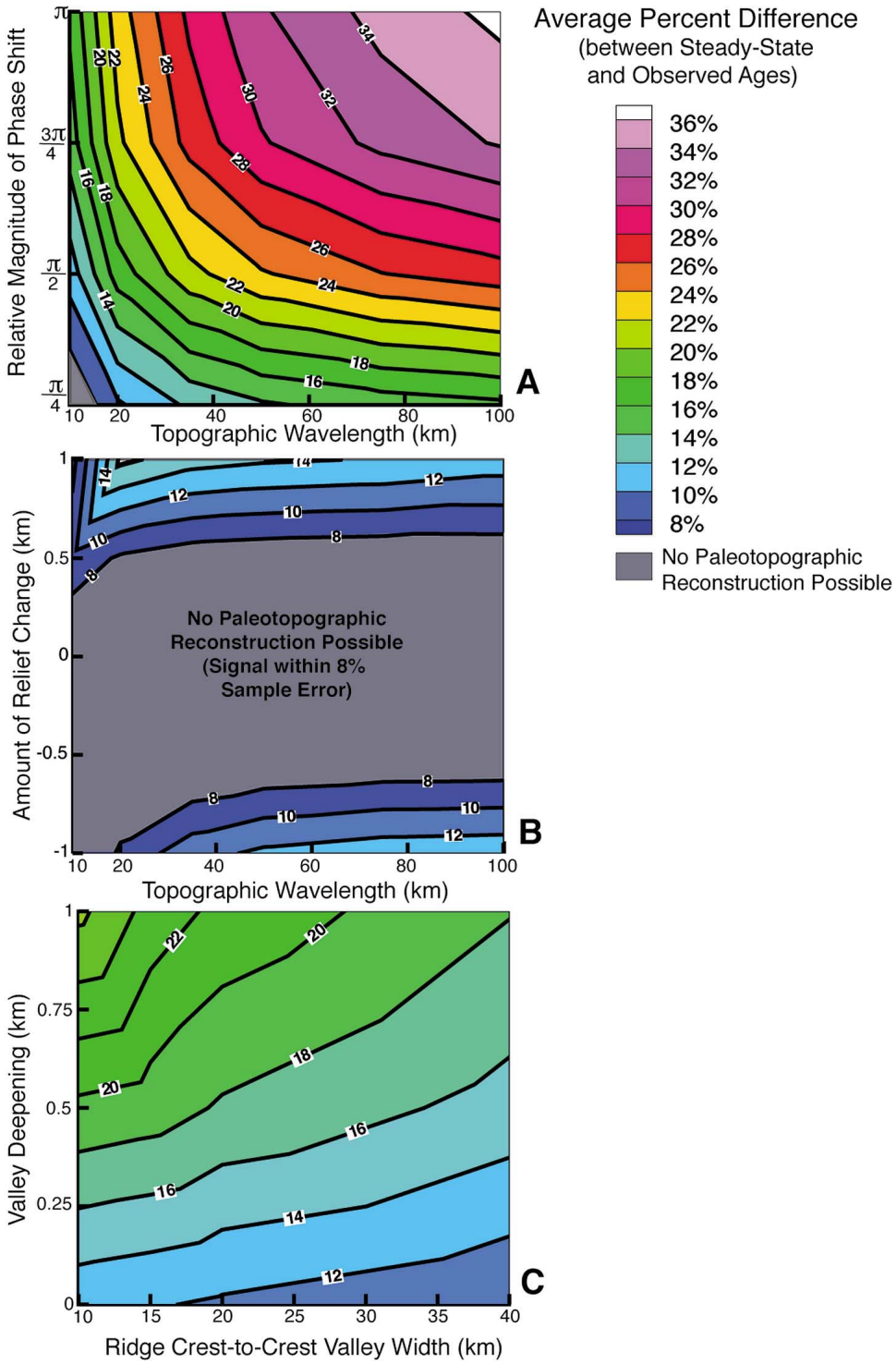

Figure 11

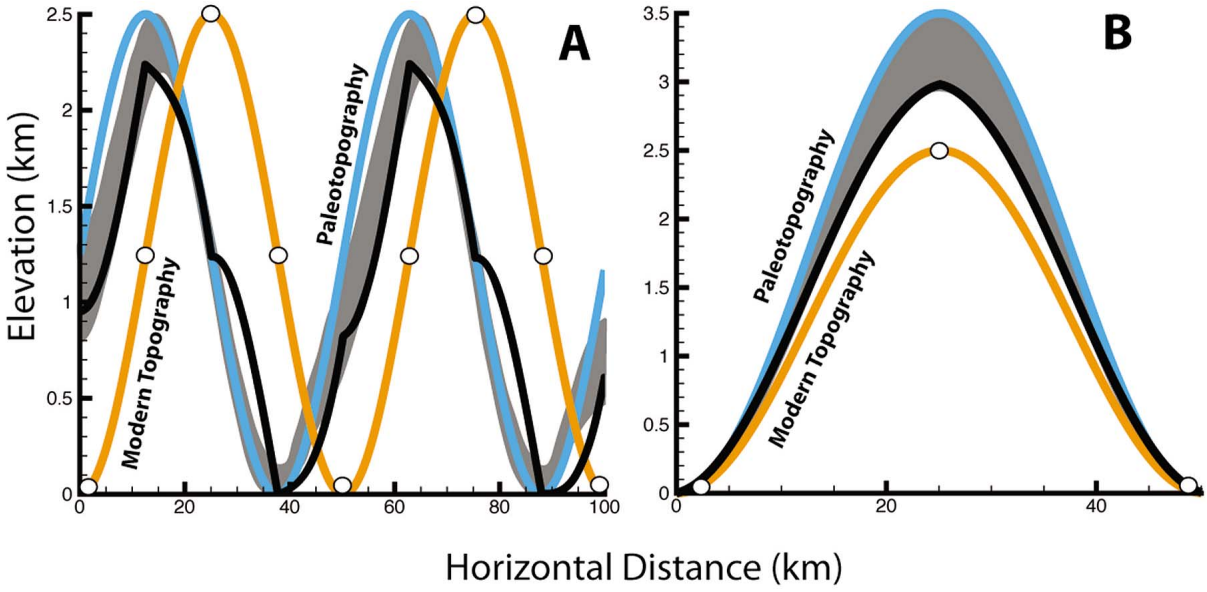

Figure 12. Elevation profiles of simulations from (a) Figure 6 (phase change of $\pi/2$, 50 km topographic wavelength) and (b) Figure 8 (relief change of 1 km, 50 km topographic wavelength) using the minimum data required to reconstruct paleotopography within sample error. Five data points (valley bottoms, ridge flanks, and ridge crest) are required to capture lateral ridge migration (Figure 12a) within 1σ error. (The somewhat peculiar shape of the topography is an artifact of interpolating the elevation correction over the number of nodes in the topography.) For relief change (Figure 12b), however, three only data points in the valleys and at the ridge peak are required to reconstruct paleotopography within 1σ error.

thermochronometry may not be sufficiently sensitive to relief change to accurately predict the magnitude of past relief and is likely to underestimate this value (e.g., Figure 8). It should also be noted that the primary difference between ages predicted for steady state topography and those predicted on topographies experiencing relief change is a change in slope of the AER (e.g., Figure 7). This change can also be caused by an increase or decrease in exhumation rate and does not necessarily indicate a change in topography. In other words, low-temperature thermochronometer data alone cannot be used to differentiate between a change relief versus a change in exhumation rate.

[37] Glacial valley evolution is simulated here as a combination of both valley widening and deepening (Figure 4c). Figure 11c shows the initial percent age difference between synthetic data and ages predicted on a steady state modern topography contoured for a range of ridge crest wavelengths. The AHe age sensitivity to valley deepening and widening is generally low to moderate, ranging between %Diff = 10.26% and %Diff = 26.51%. The highest sensitivity (e.g., %Diff = 26%) is found for model simulations where the ridge crest-to-crest distance is low and valley deepening is high (e.g., for wavelengths below 20 km and valley deepening above 0.6 km; see Figure 11c). This is caused by topography eroding from paleotopography to modern topography to an elevation close to the previous closure isotherm of the fluvial paleotopography. When the valley width is greater (e.g., ridge crest-to-crest of 40 km) this does not occur, resulting in a smaller signal in thermochronometer data. This difference does not exist when the amount of valley deepening is less than ~0.5 km. In general, glacial valley evolution produces a stronger topographic signal in AHe ages than ridge evolution-driven relief change (scenario 2), and paleotopographic reconstruction can be performed with moderate success.

[38] In all scenarios of topographic change, some amount of paleotopographic reconstruction is possible. The higher sensitivity of lateral ridge migration compared to relief change and glacial valley evolution, may be explained by the fact that topographic change is occurring at every point along the topography. In the relief change and glacial valley evolution scenarios, however, topographic change is focused on ridge crests or valley bottoms. As the percent difference between predicted and observed ages is averaged across the topography, scenarios in which part of the topography does not change (e.g., topographic relief change) will necessarily produce a smaller misfit and less signal than a scenario in which all of the topography changes (e.g., ridge migration). The conclusions drawn from the simulations presented here, then, are limited by the chosen topographic change scenarios, exhumation rates, and misfit statistics.

5.2. Minimum Data Required

[39] To assess the number of sample locations (data) required to successfully perform paleotopographic reconstruction, we repeat the simulations in Figures 6 and 8 (phase and relief change) with a limited number of sample locations. Two scenarios are considered: (1) AHe ages are taken from the valleys, at the midpoint of the ridge flanks, and at the peak of each ridge and (2) ages are taken from only the valleys and the peaks of each ridge. Figure 12 shows the results of these simulations. The location of data points used is shown on the modern topography by white circles. The resulting reconstructed paleotopography is

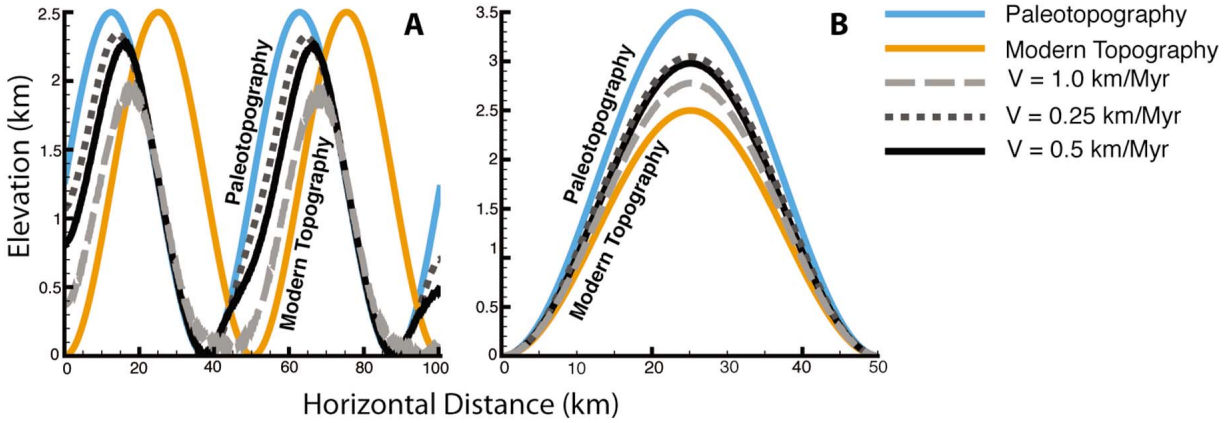

Figure 13. Elevation profiles of simulations from (a) Figure 6 (phase change of $\pi/2$, 50 km topographic wavelength) and (b) Figure 8 (relief change of 1 km, 50 km topographic wavelength) reconstructed using the following exhumation rates: 0.25 km Myr^{-1} (dark gray dashed), 0.5 km Myr^{-1} (solid black), and 1.0 km Myr^{-1} (light gray dashed). All simulations stop when the average percent difference is within the 8% sample error.

shown against the envelope of acceptable paleotopographies calculated in Figures 6 and 8. For the case of ridge migration (Figure 12a), sample locations are required in the valley, the midpoint of the ridge flank, and the ridge peak to successfully reconstruct paleotopography. The midpoint of the ridge flank is critical to capture ridge migration; when only data at the ridge peak and valley are used, the method predicts a plateau-like topography at mean elevation. In the case of relief change, however (Figure 12b), paleotopography can be successfully reconstructed using only data located in the valleys and at ridge peaks. The resulting paleotopography does underpredict the extent of paleorelief (as in other simulations), but the reconstructed paleotopography fits the suite of acceptable topographies. To capture the trend of paleotopography for phase or relief change, only five or three sample locations, respectively, are required. It is recommended that data from along the ridge flanks are included to capture the full range of possible paleotopographies as a priori knowledge of the shape of paleotopography is generally not known.

5.3. Effect of Faster and Slower Background Exhumation Rates

[40] Previous studies have suggested that the sensitivity of thermochronometer data to topographic change depends on the magnitude of the exhumation rate [e.g., *Stüwe et al.*, 1994; *Valla et al.*, 2010]. Though a detailed analysis of the effect of various background exhumation rates is beyond the scope of this study, some consideration is paid here to the effect of faster and slower background exhumation rates on the ability of the method to reconstruct paleotopography. The simulations used in Figure 6 (phase change) and in Figure 8 (relief change) are repeated with half and double the original background exhumation rate, 0.25 km Myr^{-1} and 1.0 km Myr^{-1}, respectively. Figure 13 shows the resulting reconstructed topographies using background exhumation rates 0.25 km Myr^{-1} (light gray dashed), 0.5 km Myr^{-1} (black solid), and 1.0 km Myr^{-1} (dark gray dashed) against modern and paleotopographies. The simulations with a faster exhumation rate (1.0 km Myr^{-1}) predict the paleoposition of the advancing ridge flank for the case of ridge migration (Figure 13a), but the position of the retreating ridge flank is nearly identical to the modern topography. Likewise, in both the cases of ridge migration and relief change (Figures 13a and 13b), the paleotopography predicted with the background exhumation rate of 1.0 km Myr^{-1} underpredicts the elevation of the paleoridge by approximately 0.5 km. In contrast, simulations using the slower background exhumation rate (0.25 km Myr^{-1}) result in a similar, in fact slightly more accurate, predicted paleotopography. Background exhumation rate in these instances has a clear impact on the ability of the method to successfully reconstruct paleotopography. The increased topographic sensitivity of subsurface temperatures to slower background exhumation rates has previously been noted by other studies [*Stüwe et al.*, 1994; *Valla et al.*, 2010]. A more detailed study is necessary to quantify the extent of this impact, but caution should be used when applying this method of paleotopographic reconstruction to geologic settings with a higher background exhumation rate (e.g., Taiwan, New Zealand, or the Himalaya).

5.4. Application of the Method to Coast Mountains, British Columbia

[41] The Coast Mountains are a heavily glaciated mountain range on the western margin of North America, extending ~1200 km from southern British Columbia to Alaska. Glaciation in the northern Coast Mountains began at ~9 Ma [*Denton and Armstrong*, 1969]; in the southern Coast Mountains the onset of glaciation is less well known, but is thought to have started between 2 and 8 Ma [*Clague*, 1991]. Large glaciers have been present in the Coast Mountains during both glacial and interglacial periods. The Mount Waddington region (Figures 2 and 14a), the highest elevation of the present-day range (~4 km), is presently surrounded by glaciers and has no currently known evidence for Neogene faulting [e.g., *Ehlers et al.*, 2006], with only minor faulting documented in the last 10 Myr several hundred kilometers to north of our study area [*Farley et al.*, 2001]. The region is composed of Jurassic to Eocene

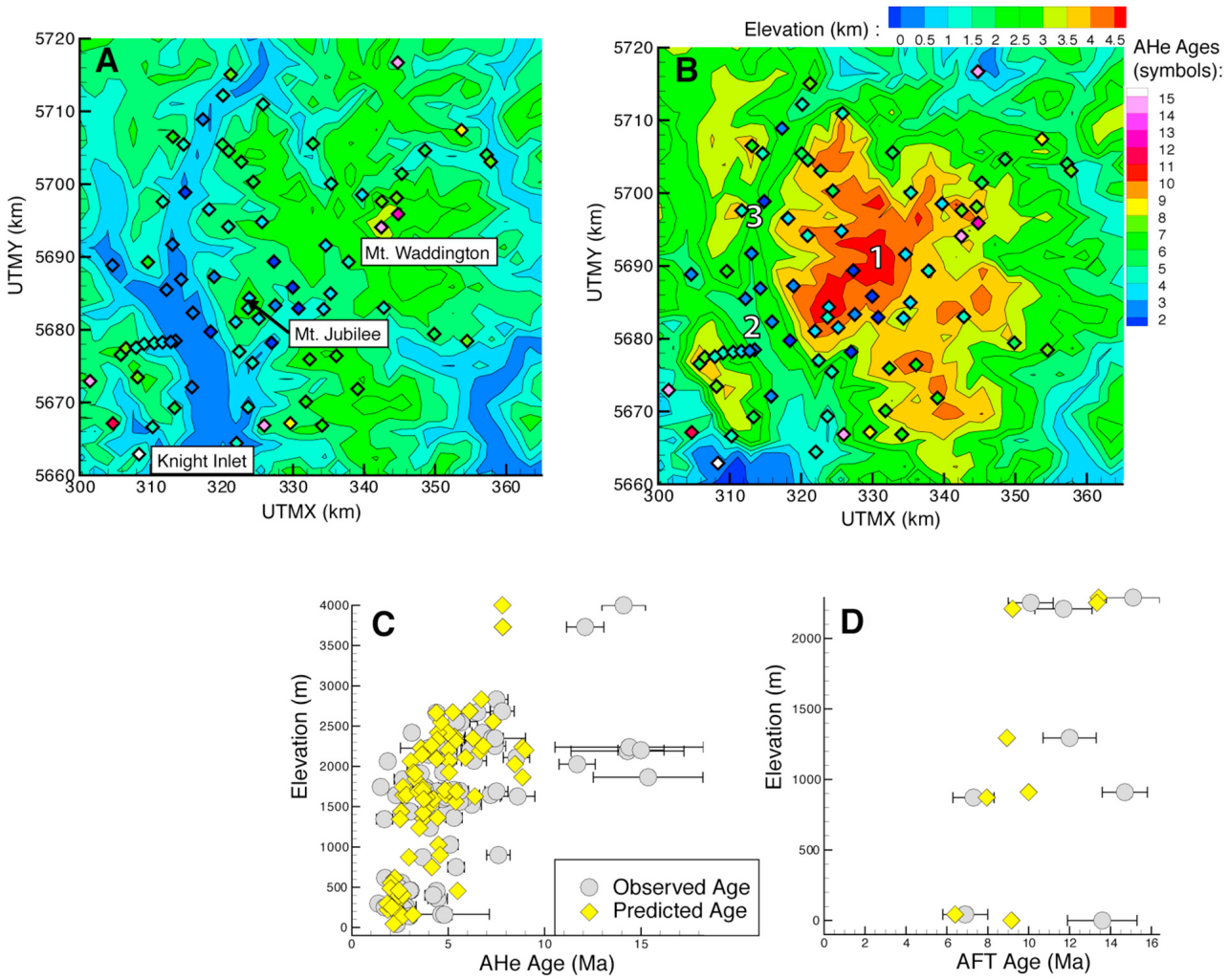

Figure 14. Results of the application of the iterative method to the Mount Waddington region of the Coast Mountains, British Columbia. (a) An aerial view of the modern topography of the study area, showing Mount Waddington, Mount Jubilee, and the Knight Inlet. AHe sample locations and ages are represented as diamonds. Note the relatively young ages (2–3 Ma) on Mount Jubilee. (b) An aerial view of the reconstructed paleotopography (topography from 50 to 1.8 Ma). This topography was reconstructed assuming a background exhumation rate of 0.3 km Myr^{-1}. Highlighted features are (1) topographic high near Mount Jubilee, which serves as an explanation for the young ages near modern day Mount Jubilee; (2) the Klinaklini valley, which has a relatively narrow valley with more gently sloped sidewalls compared to the modern topography; and (3) a drainage divide at the northeast end of the Klinaklini valley that does not exist in the modern topography. (c) AER of AHe ages for the region. Observed ages (gray circles) are shown with the measured sample uncertainty. Reconstructed ages using a transient simulation from paleotopography to modern topography are shown as yellow diamonds. This paleotopography provided an AHe age misfit reduction from %Diff = 177 to %Diff = 33%. (d) AER for AFT ages for the region. The AFT misfit reduced from %Diff = 79% to %Diff = 22% using the reconstructed paleotopography.

granodiorite and tonalite plutons and orthogneisses [*Woodsworth et al.*, 1991], which produce high-quality grains for AHe and AFT dating [*Densmore et al.*, 2007].

[42] A large thermochronometer data set of AHe and AFT ages exists for the Mount Waddington region [*Parrish*, 1983; *O'Sullivan and Parrish*, 1995; *Ehlers et al.*, 2006; *Densmore et al.*, 2007; *Densmore*, 2008]. Samples were taken from the Coast Plutonic Complex with locations ranging from sea level at Knight Inlet to 4 km at the top of Mount Waddington (Figure 14a). These cooling ages show a trend of younger ages in the center of the orogen and older ages on the flanks [*Ehlers et al.*, 2006]. Previous $^{4}He/^{3}He$ thermochronometer studies suggest an increase in glacial erosion circa 1.8 Ma [*Shuster et al.*, 2005]. Southwest of Mount Waddington, young AHe ages at relatively high elevations on Mount Jubilee suggest a possible lateral shift in the topographic high point of the range [*Ehlers et al.*, 2006]. A robust AHe age data set, a long history of glaciation, and a suggested uniform vertical (erosional) exhumation trajectory [*Parrish*, 1983] make the Coast Mountains a

Table 2. Explored Parameters and Fixed Parameters Used in the Application to the Mount Waddington Region of the Coast Mountains, British Columbia[a]

Parameter	Value
Fixed Model Parameters	
Initiation of model	50 Ma
Rock uplift begins	20 Ma
Duration of topographic evolution	1.8 Myr
Crustal thickness	40 km
Thermal conductivity	2.24 W m^{-1} K^{-1}
Specific heat capacity	956 J kg^{-1} K^{-1}
Crustal density	2700 kg m^{-3}
Mantle density	3200 kg m^{-3}
T at base of model	800°C
T at lowest elevation	10°C
Atmospheric lapse rate	6.69°C km^{-1}
Crustal heat production at surface	0.8 μW m^{-3}
e-folding depth	10 km
Mantle heat production	0.02 μW m^{-3}
Model resolution	900 × 900 m
Grid size	1230 × 1022
Topographic evolution	linear
Explored Parameters	
Uniform background exhumation rate	0.2, 0.3, 0.4, 0.5, 0.6 km Myr^{-1}

[a]Thermophysical properties were measured by *Densmore* [2008] and are averaged for the region. The variation in exhumation rate was chosen to reflect a range of plausible preglacial exhumation rates.

well-suited application site for paleotopographic reconstruction. The model application to the Coast Mountains begins with the most geologically simple scenario and assumes that background exhumation in the region is spatially uniform across a domain of evolving topography.

[43] A suite of 3-D simulations is performed using 80 AHe and 8 AFT observed ages to invert for paleotopography. AHe ages, which span the range of times suggested for the onset of glaciation in the region, are used to invert for paleotopography in the iterative method. The explored parameter in these simulations includes a range of uniform background exhumation rates between 0.2 and 0.6 km Myr^{-1}. A nonuniform (parabolic) uplift field was also explored, prompted by the older ages on the flanks of the mountain range [*Ehlers et al.*, 2006], but the results did not vary significantly from what is presented here. For brevity, the simplest scenario of uniform uplift is presented here to illustrate the approach. On the basis of $^4He/^3He$ analysis by *Shuster et al.* [2005], which suggests that rapid glacial erosion began in the Mount Waddington region at 1.8 Ma, the onset of topographic evolution in the model is set at 1.8 Ma and continues to the present. Other timings for the onset of glaciation were also considered (e.g., 2, 4, and 8 Ma) but did not provide a good fit to the data, suggesting a recent pulse of topographic change is needed to fit the observations. A 90 m digital elevation model (DEM) of the Mount Waddington region is resampled at 900 m and used as the initial topographic input (Figure 1) for the iterative scheme. Zero-flux conditions are implemented at the boundary of the DEM; a sufficiently large area was chosen (~20 km between boundaries and sample locations) for the DEM so that existing sample locations would not be influenced by topographic effects on the boundaries. Thermochronometer ages are calculated using a medium radiation damage model for AHe ages [*Shuster et al.*, 2006] based on the average U/Th concentration in the samples (eU = 32 ppm) [*Densmore*, 2008]. This level of radiation damage represents the average of the samples. Thermophysical properties were previously measured from samples by *Densmore* [2008] and are summarized along with other model parameters in Table 2. Long-term, background exhumation rates are constrained using the 8 AFT ages; if AFT ages in the final reconstruction are older than observed, the background exhumation rate is considered too slow; likewise, if the AFT ages are younger than observed, the background erosion rate is considered too fast.

[44] The iterative method reconstructs a paleotopography that provides a significant misfit reduction between predicted and observed AHe and AFT ages (Figure 14). Figure 14b shows the best fit reconstruction of paleotopography to the data. This simulation uses a uniform exhumation rate of 0.3 km Myr^{-1}. The thermochronometer age misfit is reduced from %Diff = 177% (AHe) and %Diff = 79% (AFT) for a steady state modern topography to %Diff = 33% (AHe) and %Diff = 22% (AFT) using a paleotopography evolving over 1.8 Myr to the modern topography. While the age difference is not completely minimized (see discussion below), this represents a substantial reduction in misfit.

[45] Modern topography with AHe sample locations (Figure 14a) is shown beside the reconstructed paleotopography (Figure 14b). The dominant feature visible on the reconstructed topography is the large peak near present-day Mount Jubilee. This corresponds to young AHe ages (~2–3 Ma) at relatively high elevation (~2 km) and is consistent with previous work by *Ehlers et al.* [2006], suggesting a ~16 km shift of high topography to the west of present-day Mount Waddington. This shift in the topographic high accounts for the removal of approximately 3 km of rock at up to 1.8 km Myr^{-1}. Also notable is that the Klinaklini Valley, north of Knight Inlet, has narrowed in the reconstructed paleotopography from a valley bottom approximately 5 km wide in the modern topography to approximately 2.5 km wide in the reconstructed paleotopography. The valley walls are also more gradual, suggesting a more fluvial-like valley than is currently present. Additionally, in the northeastern branch of the Klinaklini valley, there appears to be a drainage divide that no longer exists (point 3 in Figure 14b).

[46] Age elevation relationships for AHe and AFT (Figures 14c and 14d) demonstrate the relatively good fit between predicted and observed ages. AHe ages older than 10 Ma are not reproduced in the transient paleotopography to modern topography scenario. This may be an artifact of Pecube, which applies a uniform background exhumation rate across the domain. However, existing high peaks in a glaciated orogen have likely experienced little to no erosion relative to the rest of the topography. Alternatively, a spatially nonuniform background exhumation over the region may be needed to improve the fit the older ages.

[47] There are several possible reasons why our 3-D reconstruction of paleotopography (Figure 14b) does not reduce the average age difference between predicted and observed topographies below sample error (final %Diff = 33% for AHe). The iterative method is a single-parameter inversion and minimizes the age differences only by modifying paleotopography. Several other geologic processes could be active in this area that are not accounted for in the

inversion. For example, nonuniform background exhumation rate, fluid flow, magmatism, unknown sample variations in thermophysical properties, and/or variations in the He diffusion kinetics could all produce variations in observed cooling ages that our approach would be unable to minimize without additional constraints (e.g., Figures 14c and 14d).

[48] Despite these complications, the iterative method provides a significant reduction in the misfit to cooling ages (%Diff = 177% to %Diff = 33% for AHe; %Diff = 79% to %Diff = 22% for AFT) and quantifies the paleotopographic signal present in observed cooling ages. Assuming that the effects on cooling ages of other processes not accounted for in the model are minimal (e.g., faulting, fluid flow, magmatism), the reconstructed paleotopography provides interesting implications for the impact of glaciers in mountainous landscapes. Exhumation rates predicted from 1.8 Ma to present to compensate for the amount of topographic change represent a 460–600% increase on Mount Jubilee compared to the uniform preglacial rate, and a 266–400% increase in the Klinaklini Valley. These increases are relatively large compared to previously predicted increases in exhumation rates by *Ehlers et al.* [2006]. Furthermore, the predicted paleotopography suggests that glaciation has the potential to remove drainage divides and that erosion by alpine glaciers is not only focused in preexisting fluvial valleys, as evidenced by the existence and removal of the previous topographic high, but that glaciers may have a much broader impact on the orogen landscapes at intermediate and high elevations.

6. Concluding Remarks

[49] Paleotopographic reconstruction can be completed under a limited, but geomorphologically interesting, set of scenarios. Successful applications of the iterative inverse approach presented here can occur in regions without major active faulting or other significant complications and where the kinematic field is well understood. The method is best suited to landscapes experiencing low to moderate rates of background exhumation, and is not recommended for orogens experiencing high rates of background exhumation. The exploration of 2-D topographic scenarios suggests the iterative method is best applied to longer wavelength topographies (≥30 km). Paleotopographic reconstruction of short-wavelength topographies, such as individual glacial or fluvial valleys, will be limited by the low to moderate sensitivity in the AHe and AFT age data and in some cases may not be possible. The most successful applications of this method are likely in regions experiencing the lateral migration of ridges, such as mountain belts dominated by orographic precipitation or glacial headwall erosion. The utility of AHe age data to reconstruct relief change is limited and generally only applicable to regions with increases or decreases in relief greater than 0.5 km or 0.1 km Myr^{-1} (Figure 11b). While the method has limited success reconstructing preglacial fluvial valleys, reconstructing the paleotopography of large-scale glaciated landscapes could lend important insight into the behavior of glaciers in a wider region. For all topographic scenarios, it is important to note that the method will likely underpredict the amount of topographic change that has taken place, particularly in the case of relief change. The application of this method to the Coast Mountains of British Columbia suggests that alpine glaciers are capable of removing drainage divides and shifting the location of topographic highs, in addition to broadening existing valleys.

[50] Any application of the method to a new geologic region will require that the thermokinematic model be calibrated to local thermal and kinematic conditions. If there is no prior knowledge of the background exhumation rate or the timing of topographic change in the region, a suite of possible values will need to be tested, as is done in the application to the Coast Mountains. When a robust thermochronometer data set has been collected, anomalous age-elevation relationships, such as young ages at high elevation in the Coast Mountains or looped/elliptical age-elevation relationships from samples collected on both sides of a ridge can be telltale signs of topographic change. These patterns in ages can be caused by lateral ridge migration, drainage divide removal, or lateral shifting of ridges and peaks. In these cases, the single-parameter inverse technique presented here has the potential to be a useful tool in constraining transient topographies.

[51] **Acknowledgments.** This work was supported by U.S. National Science Foundation grant EAR-0724656 and German Science Foundation grant (DFG) EH329/1-1. We thank Jean Braun for providing the Pecube source code that was modified for this study. We are also grateful to Dave Whipp for assistance in modifying Pecube-D and to Glenn Woodsworth, Margi Rusmore, and Ken Farley for constructive discussions concerning the evolution of the Coast Mountains and AHe thermochronometry. We thank Jean Braun, Dimitri Lague, Jim Spotila, and Pierre Valla for constructive reviews.

References

Bao, G., Y. Dou, T. A. Ehlers, P. Li, Y. Wang, and Z. Xu (2011), Quantifying tectonic and geomorphic interpretations of thermochronometer data with inverse problem theory, *Commun. Comput. Phys.*, *9*, 129–146, doi:10.4208/cicp.090110.270410a.

Braun, J. (2002a), Quantifying the effect of recent relief changes on age-elevation relationships, *Earth Planet. Sci. Lett.*, *200*, 331–343, doi:10.1016/S0012-821X(02)00638-6.

Braun, J. (2002b), Estimating exhumation rate and relief evolution by spectral analysis of age-elevation datasets, *Terra Nova*, *14*, 210–214, doi:10.1046/j.1365-3121.2002.00409.x.

Braun, J. (2003), Pecube: A new finite-element code to solve the 3D heat transport equation including the effects of a time-varying, finite amplitude surface topography, *Comput. Geosci.*, *29*, 787–794, doi:10.1016/S0098-3004(03)00052-9.

Braun, J. (2005), Quantifying constraints on the rate of landform evolution derived from low-temperature thermochronology, in *Low-Temperature Thermochronology: Techniques, Interpretations, and Applications*, *Rev. Mineral. Geochem.*, vol. 58, edited by P. W. Reiners and T. A. Ehlers, pp. 351–374, Mineral. Soc. of Am., Chantilly, Va., doi:10.2138/rmg.2005.58.13.

Braun, J., and X. Robert (2005), Constraints on the rate of post-orogenic erosional decay from low-temperature thermochronological data: Applications to the Dabie Shan, China, *Earth Surf. Processes Landforms*, *30*, 1203–1225, doi:10.1002/esp.1271.

Braun, J., and M. Sambridge (1997), Modeling landscape evolution on geological time scales: A new method based on irregular spatial discretization, *Basin Res.*, *9*, 27–52, doi:10.1046/j.1365-2117.1997.00030.x.

Clague, J. J. (1991), Quaternary glaciation and sedimentation, in *Geology of Canada*, vol. 4, *Geology of the Cordilleran Orogen in Canada*, edited by H. Gabrielse and C. J. Yorath, pp. 421–434, Geol. Surv. Can., Ottawa.

Densmore, M. S. (2008), *Quantifying long-term glacial denudation with low-temperature thermochronology*, 186 pp., Univ. of Mich., Ann Arbor.

Densmore, M. S., T. A. Ehlers, and G. J. Woodsworth (2007), Effect of Alpine glaciation on thermochronometer age-elevation profiles, *Geophys. Res. Lett.*, *34*, L02502, doi:10.1029/2006GL028371.

Denton, G. H., and R. L. Armstrong (1969), Miocene-Pliocene glaciations in southern Alaska, *Am. J. Sci.*, *267*, 1121–1142, doi:10.2475/ajs.267.10.1121.

Dodson, M. H. (1973), Closure temperature in cooling geochronological and petrological systems, *Contrib. Mineral. Petrol.*, *40*, 259–274, doi:10.1007/BF00373790.

Ehlers, T. A. (2005), Crustal thermal processes and the interpretation of thermochronometer data, in *Low-Temperature Thermochronology: Techniques, Interpretations, and Applications*, *Rev. Mineral. Geochem.*, vol. 58, edited by P. W. Reiners and T. A. Ehlers, pp. 315–350, Mineral. Soc. of Am., Chantilly, Va., doi:10.2138/rmg.2005.58.12.

Ehlers, T. A., and D. S. Chapman (1999), Normal fault thermal regimes: Conductive and thermal heat transfer surrounding the Wasatch fault, Utah, *Tectonophysics*, *312*, 217–234, doi:10.1016/S0040-1951(99)00203-6.

Ehlers, T. A., and K. A. Farley (2003), Apatite (U-Th)/He thermochronometry: Methods and applications to problems in tectonic and surface processes, *Earth Planet. Sci. Lett.*, *206*, 1–14, doi:10.1016/S0012-821X(02)01069-5.

Ehlers, T. A., and C. J. Poulsen (2009), Influence of Andean uplift on climate and paleoaltimetry estimates, *Earth Planet. Sci. Lett.*, *281*, 238–248, doi:10.1016/j.epsl.2009.02.026.

Ehlers, T. A., et al. (2005), Computational tools for low-temperature thermochronometer interpretation, in *Low-Temperature Thermochronology: Techniques, Interpretations, and Applications*, *Rev. Mineral. Geochem.*, vol. 58, edited by P. W. Reiners and T. A. Ehlers, pp. 589–622, Mineral. Soc. of Am., Chantilly, Va., doi:10.2138/rmg.2005.58.22.

Ehlers, T. A., K. A. Farley, M. E. Rusmore, and G. J. Woodsworth (2006), Apatite (U-Th)/He signal of large-magnitude accelerated glacial erosion, southwest British Columbia, *Geology*, *34*(9), 765–768, doi:10.1130/G22507.1.

Enkelmann, E., J. I. Garver, and T. L. Pavlis (2008), Rapid exhumation of ice-covered rocks of the Chugach-St. Elias orogen, southeast Alaska, *Geology*, *36*(12), 915–918, doi:10.1130/G2252A.1.

Enkelmann, E., P. K. Zeitler, T. L. Pavlis, J. I. Garver, and K. D. Ridgeway (2009), Intense localized rock uplift and erosion in the St Elias orogen of Alaska, *Nat. Geosci.*, *2*, 360–363, doi:10.1038/ngeo502.

Farley, K. A. (2000), Helium diffusion from apatite: General behavior as illustrated by Durango fluorapatite, *J. Geophys. Res.*, *105*(B2), 2903–2914, doi:10.1029/1999JB900348.

Farley, K. A. (2002), (U-Th)/He dating: Techniques, calibrations, and applications, in *Noble Gases in Geochemistry and Cosmochemistry*, *Rev. Mineral. Geochem.*, vol. 47, edited by D. Porcelli, C. J. Ballentine, and R. Wieler, pp. 819–844, Mineral. Soc. of Am., Chantilly, Va.

Farley, K. A., M. E. Rusmore, and S. W. Bogue (2001), Post-10 Ma uplift and exhumation of the northern Coast Mountains, British Columbia, *Geology*, *29*(2), 99–102, doi:10.1130/0091-7613(2001)029<0099:PMUAEO>2.0.CO;2.

House, M. A., B. P. Wernicke, and K. A. Farley (1998), Dating topography of the Sierra Nevada, California, using apatite (U-Th)/He ages, *Nature*, *396*, 66–69, doi:10.1038/23926.

House, M. A., B. P. Wernicke, and K. A. Farley (2001), Paleo-geomorphology of the Sierra Nevada, California, from (U-Th)/He ages in apatite, *Am. J. Sci.*, *301*, 77–102, doi:10.2475/ajs.301.2.77.

Huntington, K. W., A. E. Blythe, and K. V. Hodges (2006), Climate change and late Pliocene acceleration of erosion in the Himalaya, *Earth Planet. Sci. Lett.*, *252*, 107–118, doi:10.1016/j.epsl.2006.09.031.

Insel, N., C. J. Poulsen, and T. A. Ehlers (2009), Influence of the Andes Mountains on South American moisture transport, convection, and precipitation, *Clim. Dyn.*, *35*, 1477–1492, doi:10.1007/s00382-009-0637-1.

Ketcham, R. A. (2005), Forward and inverse modeling of low-temperature thermochronometry data, in *Low-Temperature Thermochronology: Techniques, Interpretations, and Applications*, *Rev. Mineral. Geochem.*, vol. 58, edited by P. W. Reiners and T. A. Ehlers, pp. 275–314, Mineral. Soc. of Am., Chantilly, Va., doi:10.2138/rmg.2005.58.11.

Kooi, H., and C. Beaumont (1996), Large-scale geomorphology: Classical concepts reconciled and integrated with contemporary ideas via a surface processes model, *J. Geophys. Res.*, *101*(B2), 3361–3386, doi:10.1029/95JB01861.

Lachenbruch, A. H. (1970), Crustal temperature and heat production: Implications of the linear heat-flow relation, *J. Geophys. Res.*, *75*, 3291–3300, doi:10.1029/JB075i017p03291.

Lees, C. H. (1910), On the shapes of the isogeotherms under mountain ranges in radio-active districts, *Proc. R. Soc. London A*, *83*(563), 339–346.

O'Sullivan, P. B., and R. R. Parrish (1995), The importance of apatite composition and single-grain ages when interpreting fission track data from plutonic rocks: A case study from the Coast Ranges, British Columbia, *Earth Planet. Sci. Lett.*, *132*, 213–224, doi:10.1016/0012-821X(95)00058-K.

Parrish, R. R. (1983), Cenozoic thermal evolution and tectonics of the Coast Mountains of British Columbia: 1. Fission track dating, apparent uplift rates, and patterns of uplift, *Tectonics*, *2*(6), 601–631, doi:10.1029/TC002i006p00601.

Pinet, C., C. Jaupart, J.-C. Mareschal, C. Gariepy, G. Bienfait, and R. Lapointe (1991), Heat flow and structure of the lithosphere in the eastern Canadian Shield, *J. Geophys. Res.*, *96*(B12), 19,941–19,963, doi:10.1029/91JB01020.

Rahl, J. M., T. A. Ehlers, and B. A. van der Pluijm (2007), Quantifying transient erosion of orogens with detrital thermochronology from syntectonic basin deposits, *Earth Planet. Sci. Lett.*, *256*, 147–161, doi:10.1016/j.epsl.2007.01.020.

Roe, G. H., and R. S. Lindzen (2001), The mutual interaction between continental-scale ice sheets and atmospheric stationary waves, *J. Clim.*, *14*, 1450–1465, doi:10.1175/1520-0442(2001)014<1450:TMIBCS>2.0.CO;2.

Sambridge, M. (1999a), Geophysical inversion with a neighbourhood algorithm—I. Searching a parameter space, *Geophys. J. Int.*, *138*, 479–494, doi:10.1046/j.1365-246X.1999.00876.x.

Sambridge, M. (1999b), Geophysical inversion with a neighbourhood algorithm—II. Appraising the ensemble, *Geophys. J. Int.*, *138*, 727–746, doi:10.1046/j.1365-246x.1999.00900.x.

Schildgen, T. F., T. A. Ehlers, D. M. Whipp Jr., M. C. van Soest, K. X. Whipple, and K. V. Hodges (2009), Quantifying canyon incision and Andean Plateau surface uplift, southwest Peru: A thermochronometer and numerical modeling approach, *J. Geophys. Res.*, *114*, F04014, doi:10.1029/2009JF001305.

Schildgen, T. F., G. Balco, and D. L. Shuster (2010), Canyon incision and knickpoint propagation recorded by apatite $^{4}He/^{3}He$ thermochronometry, *Earth Planet. Sci. Lett.*, *293*, 377–387, doi:10.1016/j.epsl.2010.03.009.

Shuster, D. L., T. A. Ehlers, M. E. Rusmore, and K. A. Farley (2005), Rapid glacial erosion at 1.8 Ma revealed by $^{4}He/^{3}He$ thermochronometry, *Science*, *310*, 1668–1670, doi:10.1126/science.1118519.

Shuster, D. L., R. M. Flowers, and K. A. Farley (2006), The influence of natural radiation damage on helium diffusion kinetics in apatite, *Earth Planet. Sci. Lett.*, *249*, 148–161, doi:10.1016/j.epsl.2006.07.028.

Spotila, J. A., J. T. Buscher, A. J. Meigs, and P. W. Reiners (2004), Long-term glacial erosion of active mountain belts: Example of the Chugach-St. Elias Range, Alaska, *Geology*, *32*(6), 501–504, doi:10.1130/G20343.1.

Stüwe, K., and M. Hintermüller (2000), Topography and isotherms revisited: The influence of laterally migrating drainage divides, *Earth Planet. Sci. Lett.*, *184*, 287–303, doi:10.1016/S0012-821X(00)00315-0.

Stüwe, K., L. White, and R. Brown (1994), The influence of eroding topography on steady-state isotherms. Application to fission track analysis, *Earth Planet. Sci. Lett.*, *124*, 63–74, doi:10.1016/0012-821X(94)00068-9.

Thiede, R. C., J. R. Arrowsmith, B. Bookhagen, M. O. McWilliams, E. R. Sobel, and M. R. Strecker (2005), From tectonically to erosionally controlled development of the Himalayan orogen, *Geology*, *33*(8), 689–692, doi:10.1130/G21483.1.

Thiede, R. C., T. A. Ehlers, B. Bookhagen, and M. R. Strecker (2009), Erosional variability along the northwest Himalaya, *J. Geophys. Res.*, *114*, F01015, doi:10.1029/2008JF001010.

Valla, P. G., F. Herman, P. van der Beek, and J. Braun (2010), Inversion of thermochronological age-elevation profiles to extract independent estimates of denudation and relief history—I: Theory and conceptual model, *Earth Planet. Sci. Lett.*, *295*, 511–522, doi:10.1016/j.epsl.2010.04.033.

van der Beek, P. A., P. G. Valla, F. Herman, J. Braun, C. Persano, K. J. Dobson, and E. Labrin (2010), Inversion of thermochronological age-elevation profiles to extract independent estimates of denudation and relief history—II: Application to the French Western Alps, *Earth Planet. Sci. Lett.*, *296*, 9–22, doi:10.1016/j.epsl.2010.04.032.

Waples, D. W., and J. S. Waples (2004), A review and evaluation of specific heat capacities of rocks, minerals, and subsurface fluids. Part 1: Minerals and nonporous rocks, *Nat. Resour. Res.*, *13*(2), 97–122, doi:10.1023/B:NARR.0000032647.41046.e7.

Whipp, D. M., Jr., and T. A. Ehlers (2007), Influence of groundwater flow on thermochronometer-derived exhumation rates in the central Nepalese Himalaya, *Geology*, *35*(9), 851–854, doi:10.1130/G23788A.1.

Whipp, D. M., Jr., T. A. Ehlers, J. Braun, and C. D. Spath (2009), Effects of exhumation kinematics and topographic evolution on detrital thermochronometer data, *J. Geophys. Res.*, *114*, F04021, doi:10.1029/2008JF001195.

Whipple, K. X. (2009), The influence of climate on the tectonic evolution of mountain belts, *Nat. Geosci.*, *2*, 97–104, doi:10.1038/ngeo413.

Willett, S. D., and M. T. Brandon (2002), On steady states in mountain belts, *Geology*, *30*(2), 175–178, doi:10.1130/0091-7613(2002)030<0175:OSSIMB>2.0.CO;2.

Willett, S. D., F. Schlunegger, and V. Picotti (2006), Messinian climate change ad erosional destruction of the central European Alps, *Geology*, *34*(8), 613–616, doi:10.1130/G22280.1.

Woodsworth, G. J., R. G. Anderson, R. L. Armstrong, L. C. Struik, and P. van der Heyden (1991), Plutonic regimes, in *Geology of Canada*,

vol. 4, *Geology of the Cordilleran Orogen in Canada*, edited by H. Gabrielse and C. J. Yorath, pp. 493–530, Geol. Surv. Can., Ottawa.

M. S. Densmore, Department of Geological Sciences, University of Michigan, Ann Arbor, MI 48109, USA. (mdens@umich.edu)

T. A. Ehlers, Department of Geosciences, University of Tübingen, D-72074 Tübingen, Germany. (todd.ehlers@uni-tuebingen.de)

S. M. Olen, Institute of Earth and Environmental Science, University of Potsdam, D-14476 Potsdam, Germany. (solen@umich.edu)